ADAPTIVE OPTICS FOR ASTRONOMY: Principles, Performance, and Applications

Jacques M. Beckers

European Southern Observatory, D–8046 Garching bei München, Germany

KEY WORDS: telescopes, imaging, wavefront sensing, laser guide stars

1.   INTRODUCTION

1.1   *The Function of Astronomical Telescopes*

Astronomical telescopes are devices which collect as much radiation from astronomical (stellar) objects and put it in as sharp (small) an image as possible. Both collecting area and angular resolution play a role. The relative merit of these two functions has changed over the years in optical astronomy, with the angular resolution initially dominating and then, as the atmospheric seeing limit was reached, the collecting area becoming the most important factor. Therefore it is the habit these days to express the quality of a telescope by its (collecting) diameter rather than by its angular resolution. With the introduction of techniques that overcome the limits set by atmospheric seeing, the emphasis is changing back to angular resolution. This time, however, the constraint is set by the diffraction limit of the telescope so that both angular resolution and collecting power of a telescope will be determined by its diameter. Both telescope functions will therefore go hand-in-hand. Although speckle image reconstruction techniques have been successful in giving diffraction-limited images, the most powerful and promising technique for all astronomical applications is the one using *adaptive optics*. For an unresolved image, this technique puts most of the collected photons in as small an image as possible, thereby allowing better discrimination against the sky background, improving high spectral and spatial resolution spectroscopy, and enhancing inter-

13

ferometric imaging with telescope arrays. For resolved objects adaptive optics allows imaging without the complications of image reconstruction techniques applied to short-exposure, noisy images. It therefore extends diffraction-limited imaging to much fainter and complex objects.

The technique of adaptive optics is undergoing a rapid evolution which, within the foreseeable future, is expected to lead to its full implementation on astronomical telescopes. It promises to radically change the face of ground based optical astronomy in the 21st century.

1.2   What is Adaptive Optics?

Adaptive optics removes the wavefront distortions introduced by the Earth's atmosphere by means of an optical component which is introduced in the light beam and which can introduce a controllable counter wavefront distortion which both spatially and temporally follows that of the atmosphere. This optical component is generally, but not always, a mirror whose surface can be distorted. To control the mirror, the wavefront distortions have to be known. These are measured by means of a wavefront sensor using either the object under study for its measurement or a nearby stellar or laser-generated object (also referred to as natural or *laser guide stars*). In the case where the wavefront is measured with the required accuracy and spatial and temporal resolution, and in which the adaptive mirror control is perfect, the atmospheric effects are removed and the telescope will give a diffraction-limited image. The application of adaptive optics to astronomical telescopes therefore requires the development of expensive, complex opto-mechanical devices and their control systems. Since astronomical requirements coincide to a large extent with similar requirements elsewhere (e.g. military, laser beam control), astronomers profit from the rather sizable investments already made. Thus we might hope to reach our goal of diffraction-limited imaging with large telescopes within the limited budgets available to astronomy.

1.3   Terminology

1.3.1   ACTIVE AND ADAPTIVE OPTICS   It is important to distinguish between "Adaptive Optics" and "Active Optics." The latter term is now commonly used to describe ways of controlling the wavefront distortions in a telescope introduced by mechanical, thermal, and optical effects in the telescope itself (Wilson et al 1987). Since these effects vary on a rather long time scale, Active Optics is rather slow as compared to Adaptive Optics whose purpose it is to compensate for the rapidly varying atmospheric wavefront distortions ("seeing"). Astronomical Adaptive Optics uses bandwidths in the vicinity of 10 to 1000 Hz; Active Optics works at less than 1 Hz. Because of this high bandwidth Adaptive Optics has to use

small mirrors located at an image of the pupil, whereas the Active Optics on, for example, the ESO-NTT and VLT telescopes and on the Keck telescope uses the large primary mirrors themselves for wavefront correction.

1.3.2   ISOPLANATIC ANGLE   In this review I will use the term "isoplanatic angle" in a broader sense than commonly used. Commonly it refers to the distances on the sky over which the wavefront distortions, and hence the images, are for all practical purposes the same. In the broader definition I will use it in the form of e.g. "the isoplanatic angle for image motion," referring to the distances over which the image motions are the same (also called by some the "isokinetic angle"). Without the qualifier the term will be used as commonly defined.

1.3.3   GUIDE STARS   I will use the term "guide stars" for the objects used for measuring the atmospheric wavefront distortions, including, but not restricted to, wavefront tilts. They can be either natural or laser guide stars. Natural guide stars can include such nonstellar objects as the Galilean satellites. Some astronomers, however, prefer to refer to laser guide stars as "laser beacons" and reserve the term "guide stars" to the objects used for autoguiding the telescopes.

1.4   Scope of this Review

The amount of literature on adaptive optics is extensive, and growing very rapidly. It covers applications relating to military surveillance, laser beam ("directed energy") control, nuclear fusion, and solar and nighttime astronomy. It covers widely different disciplines ranging from sophisticated opto-mechanical systems, wavefront estimation methods, atmospheric optics, atmospheric structure, performance analysis, and rapid control techniques, to the evaluation of how it functions in the given application environment. I do not attempt to cover the full range of demonstrated expertise in this review, nor do I attempt to give a full bibliography on this topic, except where the specific astronomical application is concerned. Instead I focus on the applications to astronomy— solar and nighttime. A number of other monographs and review papers on the topic have recently been published or are in preparation (Merkle 1991, Tyson 1991). I refer the reader to those for a more extensive description. Other discussions dealing with the general role of adaptive optics in large astronomical telescopes can be found in Beckers (1987a), Beckers & Goad (1988), Beckers & Merkle (1989a), Fontanella (1985), Fontanella et al (1991), Hardy (1981, 1989, 1991), Kern (1990), Merkle (1989b), Merkle & Beckers (1989), and Roddier (1992b).

## 2.   HISTORICAL BACKGROUND

2.1   Babcock's Original Concept

The concept to use adaptive optics for compensating atmospheric seeing originated with Horace W. Babcock in 1953 (Babcock 1953, 1958, 1990, 1992; Hardy 1991). Although that initial paper deals with its application to astronomical imaging at visible wavelengths, it appears to be the first description of a much broader discipline which was to find its application to military, laser power, medical (ophthalmology), and probably other fields. The Babcock paper is quite remarkable in its completeness. In addition to describing the concept (Figure 1), Babcock suggests a way of measuring the atmospheric wavefront distortions and proposes a concept for the adaptive mirror. He describes the small isoplanatic patch size ("a few seconds of arc") over which the image will be corrected and discusses the need for high temporal resolution and the consequent limitation to stars brighter than 6.3 for wavefront sensing.

2.2   Early Efforts Toward Astronomical Adaptive Optics

Following Babcock's 1953 suggestion, adaptive optics was pursued, in parallel but independently, for astronomical and military applications. The latter were well funded, but mostly classified and unavailable for astronomical use. Budgets for technology developments in astronomy being restricted, progress in implementing Babcock's concept has been very slow. Up to the mid–1980s attempts aimed at applying adaptive optics to astronomical telescopes have been limited to the first attempts by Buffington and collaborators in the mid–1970s (Buffington et al 1977a,b) and later by Hardy (Hardy 1978, 1980, 1987; Hardy et al 1977). The former used a one-dimensional, 6-element segmented mirror with segment piston control which used only dithering of the mirror segments combined with an optimizing criterion for the stellar images. The latter used a two-dimensional, 21-actuator continuous surface deformable mirror combined with a shearing interferometer wavefront sensor on both stellar and solar images. The results of these tests were both encouraging, in demonstrating the concept, and discouraging, in making the complexity of adaptive optics systems and its high cost very clear to astronomers. In addition the applicability of adaptive optics to bright stars only, led to little enthusiasm among most astronomers.

2.3   Current Efforts

A number of factors have led to the recent surge in interest in adaptive optics for astronomical telescopes: (a) the attainment of the quantum limits of astronomical panoramic detectors which led to a resurgence of interest
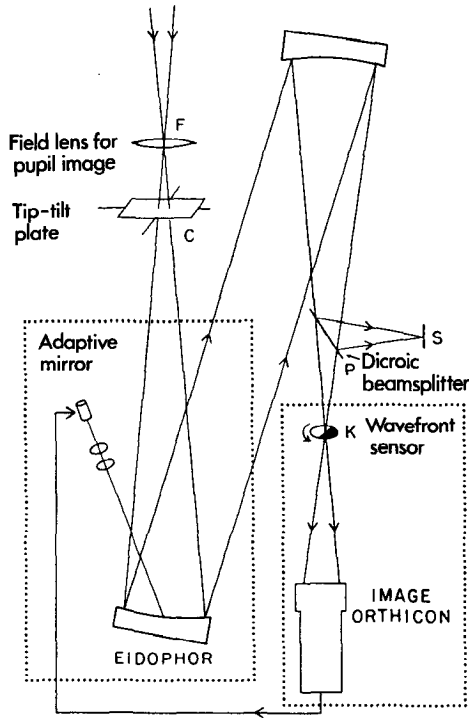
Figure 1   Adaptive optics concept as originally proposed by Babcock. Although the hardware used is different in today's systems, the principle remains unchanged. *F* images the entrance pupil onto the adaptive mirror (in this case the Eidophor). The shape of the adaptive mirror is servo-controlled by a wavefront sensor (in this case a rotating knife edge device *K*) which follows a beamsplitter *P* which sends the other part of the light to the astronomer *S*. The Tip-tilt plate *C* removes the overall image motion. (Adapted from Babcock 1953.)

in the construction of large telescopes with good imaging quality as the next natural frontier of astronomical telescope capabilities to be conquered; (*b*) the realization that many of the complexities and limitations of adaptive optics disappear at infrared wavelengths (Beckers 1987b; Beckers & Goad 1987; Beckers et al 1986; Roddier & Léna 1984; Woolf 1982, 1984; Woolf & Angel 1980). In the infrared both the number of adaptive elements and the required temporal control frequencies decrease. Locating telescopes at good seeing sites and efforts to reduce manmade seeing result in an additional decrease in complexity. The isoplanatic patch size which increases in the IR, combined with polychromatic wavefront sensing, gives access to a large fraction of the sky when using natural guide stars for

wavefront sensing. The recent availability of IR panoramic detectors has also contributed. Finally, (c) the invention of bright laser guide stars for wavefront sensing has removed the limitation in sky coverage at all wavelengths, including the visible (Feinlieb 1982, Foy & Labeyrie 1985, Fugate et al 1991, Happer & MacDonald 1982, Primmerman et al 1991).

Table 1 summarizes recent, current, and planned efforts to implement adaptive optics on astronomical telescopes (see also Beckers & Merkle 1989b, Hardy 1991). I do not include the many devices currently being built which rely solely on rapid guiding ("Tip-Tilt") of stellar images even though they would be considered by some as (rudimentary) adaptive optics systems. In addition to the adaptive optics systems listed in Table 1 there are a number of military systems that are being used on astronomical targets like the US Lincoln Laboratory SWAT system at Firepond, MA (241 actuators on a $D = 120$ cm telescope; see Murphy 1992), the USAF Phillips Laboratory Starfire Optical Range system at Albuquerque, NM (241 actuators on a $D = 150$ cm telescope; see Fugate 1992b, Fugate et al 1991, 1992). A number of other adaptive optical systems are in the early planning stages, and the listing in Table 1 is therefore likely to change rapidly.

3.   WAVEFRONT DISTORTION BY THE ATMOSPHERE

It is not within the scope of this review to go into the details of wavefront propagation and image formation through the turbulent, refractive atmosphere. In this section I will summarize only the resulting wavefront distortions to the extent that they are relevant to the implementation of adaptive optics. I refer to other excellent reviews for a more detailed description (Roddier 1981 1987, 1989; Woolf 1982).

It is common to rely on the work by Tatarski (1961) for the propagation of waves in an atmosphere with fully developed turbulence characterized by the eddy decay from larger to smaller elements in which the largest element L_u (the "upper scale of turbulence") is the scale at which the original turbulence is generated (Kolmogorov 1941). In addition there is a lower scale of turbulence L_l, set by molecular friction, at which the eddy turbulence is converted into heat. It is very small and is commonly ignored. It is convenient to describe the behavior of properties of such a turbulent field statistically in the form of its *structure function* $D(\rho)$. For the temperature, the (three-dimensional) structure function for Kolmogorov turbulence equals

$$D_T(\rho) \equiv \langle |T(\mathbf{r}+\rho) - T(\mathbf{r})|^2 \rangle_r K^2, \qquad (1)$$

which is the variance in temperature between two points a distance ρ apart. For Kolmogorov turbulence $D_T(\rho)$ equals

$$D_T(|\rho|) = C_T^2 |\rho|^{2/3} K^2, \tag{2}$$

where C_T^2 is commonly referred to as the *structure constant* of temperature variations. Temperature variations in the atmosphere result in density variations and hence in variations in the refractive index n. So, similar to the structure function and structure constant of the temperature there is a structure function and constant for the refractive index:

$$D_n(|\rho|) = C_n^2 |\rho|^{2/3}, \tag{3}$$

where

$$C_n = 7.8 \times 10^{-5}(P/T^2)C_T, \tag{4}$$

with P in millibars and T in degrees Kelvin.

There is little dispute about the validity of the Kolmogorov turbulence structure at small spatial scales of less than L_u. There is, however, substantial disagreement about the size of L_u. Balloon observations by Vernin (Coulman & Vernin 1991; Tallon et al 1992a,b) show large variations in C_T^2 on the scale of a few meters in height and anisotropies on the scale of a meter. Such variations would be consistent with L_u values of the order of a few meters. Some observations of the two-dimensional structure function $D_\phi(x)$ of the stellar wavefront phases incident on the telescope (Section 3.1.1) show a behavior consistent with a much larger L_u (up to kilometers according to Colavita et al 1987), but other observations are consistent with L_u values near 5 to 15 meters (Bester et al 1992a,b; Rigaut et al 1991). It is likely that L_u is generally not a unique quantity anyway, and that turbulent energy is fed into the atmosphere at many different scales including surface heating, high shears in atmospheric wind profiles, and the telescope environment. Although the details of the atmospheric physics per se are not of particular interest to adaptive optics, the resulting effects on the wavefront are—especially the structure function of the wavefront both for the total atmosphere and for different atmospheric layers, as well as its temporal variation. For large telescopes the structure function is normally accepted to be close to that predicted by Tatarski/ Kolmogorov.

3.1   Spatial Wavefront Structure at Ground Level

The stellar wavefront incident on the telescope has spatial variations both in phase and amplitude (both combined in the "complex amplitude"). Of these the phase variations are the most important in image formation and seeing.

Table 1 Recent, current, and planned efforts in astronomical adaptive optics

Location (name)	Application	Lambda[1]	Mirror type	Number of elements	Wave-front sensor[2]	References[3]
Lockheed/SPO	Solar	visible	segmented tip-tilt/pistoned	19	H-S	Acton, 1989, Acton & Smithson, 1991,1992, Smithson et al.,1984, Title et al., 1987
NOAO[4]	Stellar	NIR	continuous pistoned	37/55	H-S	Beckers, 1987c,1988b, Beckers et al., 1986, Goad & Beckers, 1989
ESO/France (COME-ON)	Stellar	NIR	continuous pistoned	19	H-S	Fontanella et al., 1988, Kern et al.,1988,1989a,b ,1990a,b, Merkle et al., 1991a, Rigaut et al., 1991,1992d, Rousset et al., 1990a,b
Johns Hopkins U[5]	Stellar[7]	visible	membrane mirror	61/91	CS	Clampin et al., 1991, Durrance & Clampin, 1989
Durham (MARTINI)[5]	Stellar	visible	segmented tip-tilt	6	H-S	Doel et al., 1991a,b, 1992, Sharples et al., 1992
ESO/France (COME-ON PLUS)[5]	Stellar	NIR	continuous pistoned	52	H-S	Gendron et al., 1991, Rousset et al., 1992b
U. of Hawaii	Stellar	NIR	continuous curvable	7/13	CS	Graves & McKenna, 1991, Graves et al.,1992, Roddier et al., 1987, 1991a,b

NOAO/SPO[5]	Solar	visible	continuous pistoned	61	SUN	Dunn, 1987a, 1989, 1990, Dunn et al., 1991
U. Chicago (ChAOS)[5]	Stellar	NIR	various planned	156	SI	Kibblewhite & Wild, 1992, Kibblewhite, 1992a,b
Mt Wilson (60"/ACE)[5]	Stellar	Visible & NIR	continous pistoned	69	H-S	Greenwood (priv. comm.), Shelton (priv. comm.)
CFHT (BONNETTE)[5]	Stellar	visible & NIR	continuous pistoned	44	CS	Arsenault & Salmon, 1992
ESO/VLT[6]	Stellar	NIR	continuous pistoned	256	H-S	Merkle, 1986, 1987b,c, 1988, Merkle, 1992b, Merkle & Hubin, 1991, Merkle et al., 1991b
LEST[6]	Solar	visible	continuous pistoned	200	SUN	Dunn, 1987b,c, von der Lühe, 1983

[1] Visible = 400 to 900 nm; NIR is 1 to 5 μm.
[2] H-S = Hartmann Shack Sensor, CS = curvature sensor, SI = shearing interferometer, SUN = sensing on solar granulation or sunspots.
[3] Includes only limited number of descriptive references.
[4] Discontinued due to a lack of support.
[5] Effort being implemented.
[6] Efforts in planning phase.
[7] Coronography.

3.1.1 PHASE VARIATIONS
The phase structure function at the entrance of the telescope for Kolmogorov turbulence is

$$D_\phi(x) = \langle |\phi(y+x) - \phi(y)|^2 \rangle_y = 6.88 r_o^{-5/3} x^{5/3} \, \text{rad}^2, \tag{5}$$

where coherence length r_o (the "Fried parameter") which depends on the wavelength (λ) and zenith distance (ζ) is given by

$$r_o(\lambda, \zeta) = 0.185 \lambda^{6/5} \cos^{3/5} \zeta \left(\int C_n^2 \, dh \right)^{-3/5}. \tag{6}$$

When not otherwise indicated the Fried parameter r_o in this review (and generally elsewhere) refers to $r_o(0.5 \, \mu\text{m}, 0°)$. The seeing-dominated image size d (FWHM) in a telescope relates to r_o as $d \approx \lambda/r_o$ for $r_o <$ telescope diameter D and otherwise it equals λ/D.

Although the equations given above are generally taken to be good representations of the wavefront for telescopes of modest size, there is a still ongoing debate as to what the maximum distance x is for which Equation (5) is a good approximation. Phase difference measurements with optical interferometers as a function of time t should follow a similar behavior $[D(t) = \text{constant } t^\alpha]$, but although Colavita et al (1987) find $\alpha = 5/3$ for Kolmogorov turbulence for times corresponding to distances of a kilometer and larger, Bester et al (1992a,b) find that under good seeing conditions $\alpha \approx 1$ gives a better representation of their observations made at the same site (Mt. Wilson). The Bester et al measurements refer to baselines as short as 4 meters, so that their results indicate major deviations from Kolmogorov turbulence already for values of x less than the 8–10 meter diameters D of modern large telescopes. If so, the large-scale phase variations are smaller than generally assumed, including those in this review, which are based on $L_u > D$.

3.1.2 AMPLITUDE VARIATIONS
Amplitude/intensity variations across the telescope aperture (also called scintillation) contribute much less to image quality degradation than phase variations and are therefore generally ignored in the planning and evaluation of adaptive optics systems. Roddier & Roddier (1986) showed that scintillation does contribute to the quality of image restoration at the $\approx 15\%$ level at visible wavelengths (0.5 μm), decreasing rapidly towards longer wavelengths (3% at 2.2 μm). Except for that paper I am not aware of any other publication dealing with the effect of amplitude variations on adaptive optics.

3.1.3 MODAL REPRESENTATIONS OF THE WAVEFRONT
In describing the wavefront for a circular aperture like a telescope it is often useful to express the phase variations in terms of the set of the orthogonal Zernike

polynomials $Z_j(n,m)$ in which n is the degree of a radial polynomial and m the azimuthal frequency of a sinusoidal/cosinusoidal wave. Noll (1976) gives normalized versions for $Z_j(n,m)$ in which the normalization is done in such a way that the RMS value of each polynomial over the circle equals 1. Table 2 lists the lower order terms of Z_j together with their meaning and the mean square residual amplitude Δ_j in the phase variations at the telescope entrance caused by Kolmogorov turbulence after removal of the first j terms . For large j one has approximately:

$$\Delta_j \approx 0.2944 j^{-0.866}(D/r_o)^{5/3} \, \text{rad}^2. \tag{7}$$

From Table 2 one derives for the RMS phase variation ϕ_{RMS} across a circular aperture without any correction:

$$\phi_{RMS} = 0.162(D/r_o)^{5/6} \, \text{waves}, \tag{8}$$

and after tilt correction in both directions only

$$\phi_{RMS} = 0.053(D/r_o)^{5/6} \, \text{waves}. \tag{9}$$

Most of the phase variations can therefore be removed by simple rapid guiding methods. For small wavefront disturbances, the fractional decrease $(1-SR$, where SR is called the "Strehl Ratio") in the central intensity from a perfect diffraction-limited image equals

$$1 - SR \approx \Delta \approx 1 - \exp(-\Delta), \tag{10}$$

which are referred to as the Maréchal and the extended Maréchal approxi-

Table 2 Modified Zernike polynomials and the mean square residual amplitude Δ_j (in rad^2) for Kolmogorov turbulence after removal of the first j Zernike polynomials[a]

Z_j	n	m	Expression	Description	Δ_j	Δ_j-Δ_{j-1}
Z_1	0	0	1	constant	1.030 S	
Z_2	1	1	$2r\cos\varphi$	tilt	0.582 S	0.448 S
Z_3	1	1	$2r\sin\varphi$	tilt	0.134 S	0.448 S
Z_4	2	1	$\sqrt{3}(2r^2-1)$	defocus	0.111 S	0.023 S
Z_5	2	2	$\sqrt{6}r^2\sin2\varphi$	astigmatism	0.0880 S	0.023 S
Z_6	2	2	$\sqrt{6}r^2\cos2\varphi$	astigmatism	0.0648 S	0.023 S
Z_7	3	1	$\sqrt{8}(3r^3-2r)\sin\varphi$	coma	0.0587 S	0.0062 S
Z_8	3	1	$\sqrt{8}(3r^3-2r)\cos\varphi$	coma	0.0525 S	0.0062 S
Z_9	3	3	$\sqrt{8}r^3\sin3\varphi$	trifoil	0.0463 S	0.0062 S
Z_{10}	3	3	$\sqrt{8}r^3\cos3\varphi$	trifoil	0.0401 S	0.0062 S
Z_{11}	4	0	$\sqrt{5}(6r^4-6r^2+1)$	spherical	0.0377 S	0.0024 S

[a] r = distance from center circle; φ = azimuth angle; $S = (D/r_o)^{5/3}$.

mations respectively (Δ in rad^2). For SR = 80% this implies $D = 0.4\ r_o$ without any correction at all and $D = 1.4\ r_o$ with tilt correction alone. For $D/r_o = 60$ (e.g. an 8 meter telescope with 0.75 arcsec seeing), according to Equation (7) it will take the correction of the first 3640 Zernike terms to reach SR = 80%. A more detailed analysis of the effects of the successive removal of an increasing number of Zernike polynomials on the residual structure function and on the so-called Strehl Resolution R can be found in the paper by N. Roddier (1990). The Strehl Resolution R is related to the Strehl Ratio SR. Both refer to the central intensity in the image. The Strehl Ratio, however, is normalized to the diffraction-limited performance of the telescope; R per se is not normalized, but is frequently used in the ratio R/R_{max}. This effectively normalizes the Strehl Resolution to the central intensity R_{max} of an image uncorrected for atmospheric seeing obtained with an infinitely large telescope (no diffraction) (see e.g. Roddier et al 1991b).

3.2 Variation of Wavefront Distortions with Height

3.2.1 C_n^2 VARIATIONS   Figure 2 reproduces the variation of the average value of C_n^2 with height as given by Hufnagel (1974) and Valley (1980) and extrapolated to low altitudes for day and night conditions. The actual $C_n^2(h)$ profile varies from site to site and from time to time. In addition the curve in Figure 2 does not show the very rapid fluctuations in C_n^2 with height observed in the balloon flights referred to already in Section 3. Figure 2 should therefore only be used as an approximation. One often distinguishes three layers in the $C_n^2(h)$ profile: the "surface layer" near the telescope (between about 1 to 20 meters) subject to e.g. wind-surface interactions and manmade seeing, the "planetary boundary layer" up to ≈ 1000 meters subject to the diurnal solar heating cycle, and the "free atmosphere" above this. The increase of C_n^2 at $h \approx 10$ km is related to the high wind shear regime at the tropopause. Above it the refractive index variations rapidly decrease, with an effective upper limit to atmospheric seeing occurring at $h \approx 25$ km.

3.2.2   THE ISOPLANATIC ANGLE   The isoplanatic angle θ_o is commonly defined as the radius of a circle in the sky over which the atmospheric wavefront disturbances, and their resulting instantaneous (speckle) point-spread-functions, can be considered identical. A good approximation for θ_o is

$$\theta_o = 0.314 r_o / H, \tag{11}$$

where H is the average distance of the seeing layer (Fried 1982), or
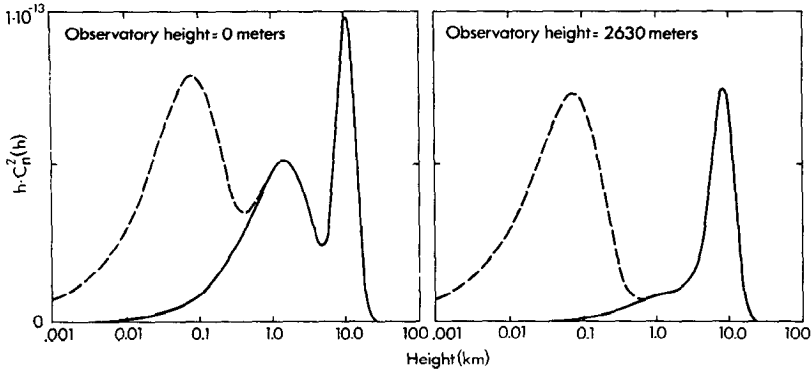
Figure 2   Average C_n^2 profile with local height h_L (in km). (*Left*) Profile for a sea level site. (*Right*) Profile for a 2630 meter high mountain site. The solid curve follows the expression given by Valley (1980) for height h above sea level: $C_n^2 = [2.05 \times 10^{-23} \cdot h^{10} \cdot \exp(-h) + 0.93 \times 10^{-16} \cdot \exp(-h/1.5)]$ $m^{-2/3}$. It ignores near ground, local seeing. It is scaled to give 0.5 arcsec seeing at $= 0.55$ μm at sea level. The dashed line corresponds to $C_n^2 = (2.17 \times 10^{-15} + 5 \times 10^{-17} \cdot h_L^{-2/3}) \cdot \exp(-h_L/0.08)$ which also results in 0.5 arcsec seeing by itself. It approximates this local nighttime seeing. For the sea level site the resulting seeing is 0.76 arcsec; for the mountain site 0.63 arcsec. For daytime condition the local seeing will be worse. The $h \cdot C_n^2$ vs log h presentation was chosen to better visualize the contributions of the different heights to r_0.

$$H = \sec \zeta \left(\int C_n^2 h^{5/3} dh \middle/ \int C_n^2 dh \right)^{3/5}. \tag{12}$$

At this distance the Strehl Ratio has decreased by an amount depending on D/r_0. For $D/r_0 = 5, 10, 20, 50, 100$, and ∞ the Strehl Ratio decreases to respectively 71, 62, 56, 49, 47, and 36% (Humpheys et al 1992). Consistent with this, Roddier & Roddier (1986) found a Strehl Ratio decrease to 45% for large D/r_0.

Sometimes the term isoplanatic patch is used in a broader sense to refer, for example, to the distance over which image motions are practically identical (as compared to their seeing-dominated width). In that case it is useful to talk about the "isoplanatic patch for image motion" θ_{motion} which is $\approx 0.3 \, D/H$. For $r_0 = 13.3$ cm (0.75 arcsec seeing at 0.5μm), $D = 8$ meters and $H = 5000$ meters, θ_0 equals 1.7 arcsec but θ_{motion} equals 100 arcsec. θ_{motion} has also been referred to as the "isokinetic patch" size. For diffraction-limited images the isoplanatic patch size for image motions is, of course, again much smaller (Chassat 1989; Chassat et al 1989a,b).

3.3   Temporal Variation of the Wavefront

The temporal variation of the wavefront is predominantly determined by the wind velocities at the different heights in the atmosphere since the turbulent elements responsible for the seeing live longer than the time it takes for them to move across their diameter. These wind velocities, typically $V_{\text{wind}} = 10$ m/sec, frequently reach 30 m/sec and higher at the ≈ 12 km tropopause layer. Since the wind directions and velocities vary with height, the temporal behavior of the wavefront is complex and hard to characterize. Typical time scales are

$$\tau_o \approx 0.314 r_o / V_{\text{wind}} \tag{13}$$

or 0.004 sec for the wavefront changes (Parenti 1992a,b; Parenti & Sasiela 1992) and $\tau_{\text{motion}} \approx 0.314 \, D/V_{\text{wind}} = 0.25$ sec for image motion. For wind velocities $v(h)$ varying with height the average wind velocity is given by

$$V_{\text{wind}} = \left(\int C_n^2 v^{5/3} dh \Big/ \int C_n^2 dh \right)^{3/5}. \tag{14}$$

The quantity $f_o = 1/\tau_o$ is closely related to the so-called Greenwood Frequency f_G which is often used in the specification of adaptive optics control systems (Greenwood 1977, Greenwood & Fried 1976). It is generally taken to be

$$f_G = 0.43 V_{\text{wind}}/r_o = 0.135 f_o. \tag{15}$$

4.   THE ASSESSMENT OF THE WAVEFRONT DISTORTION

Since it is impossible to compare directly the wavefront incident on the atmosphere interferometrically with that reaching the telescope one has to resort to measurements that assess the (spatially) differential wavefront distortions within the telescope pupil. Mostly, measurements of the wavefront gradients (tilts) are used. Other ways of assessing the wavefront using wavefront curvature analysis and neural nets are also being explored. The most important quality criterion for wavefront sensors for astronomical applications is of course their sensitivity for faint sources. Astronomical wavefront sensors using stellar signals therefore have to work broadband, in white light. I summarize here the methods used or proposed. For a more detailed discussion of wavefront sensing see Chapter 5 in the monograph by Tyson (1991).

4.1 *Wavefront Tilt Measurements*

4.1.1 FOUCAULT/KNIFE-EDGE WAVEFRONT SENSOR
Babcock (1953) proposed using the common knife-edge test to measure wavefront tilts (Figure 1). The knife edge is placed in the stellar image. To a good approximation the intensity distribution in the following pupil image then represents the wavefront gradients/tilts in a direction at right angles to the knife edge. By splitting the stellar image into two and using two knife edges in orthogonal directions the full wavefront tilt is measured. The same measurement can be made by rapidly rotating the knife edge around the stellar image. Improvements of this technique have been suggested (Goad et al 1986), but it does not appear that this method of wavefront sensing is presently favored.

4.1.2 SHEARING INTERFEROMETER WAVEFRONT SENSORS
By laterally shifting (or shearing) the wavefront and mixing it with itself, interference patterns are obtained which correspond to the wavefront tilt in the shear direction. Since the distance of the fringes are proportional to the wavelength used, gratings are commonly used to obtain an amount of shearing which is also proportional to the wavelength, thus resulting in the desired broadband, white-light signal. As is the case with the knife-edge sensor, it is necessary to make two orthogonal measurements to assess the full wavefront tilt. This method has been commonly used in military systems using a rotating radial grating followed by a detector array in a pupil image (Hardy 1978, 1982; Hardy & MacGovern 1987; Hardy et al 1977; Koliopoulos 1980).

4.1.3 HARTMANN-SHACK WAVEFRONT SENSORS
The Hartmann-Shack sensors (see Figure 3) are the most commonly used in astronomy. They are an improved version of the classical Hartmann test proposed by Shack & Platt (1971). The Hartmann screen in the pupil is replaced by an array of small lenslets in an image of the pupil. The lenslet array forms an array of images whose positions are measured to give the full vectorial wavefront tilt in the areas of the pupil covered by each lenslet. The advantage of the lenslet modification is in enhanced sensitivity since almost all the light collected is used for wavefront measurement. In addition, it is not necessary to divide the light into two, as is the case for the knife-edge and shearing interferometer device so that all photons per subaperture can be used to measure the wavefront tilt. A description of some Hartmann-Shack wavefront sensors can be found e.g. in Allen et al (1987), Gaffard & Boyer (1989), Rousset et al (1987), and Séchaud et al (1991).

The dimensions of the lenslets is often taken to correspond approximately to r_o. For otherwise perfect wavefront correction this results in
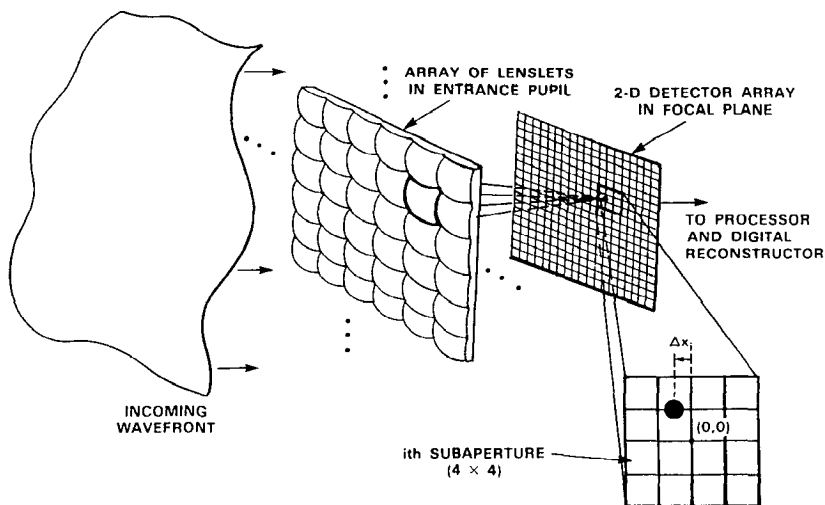
Figure 3 Principle of Hartmann-Shack wavefront sensor. The lenslets array produces an array of star images on the 2-dimensional detector array (generally a CCD or Intensified CCD). Tilt variations in the incoming, distorted wavefront result in position variations $(\Delta x, \Delta y)$ of the star images on the detector. These are measured and fed to a digital processor which reconstructs the wavefront distortions. (From Murphy 1992; reprinted with permission of Lincoln Laboratory, MIT, Lexington, MA.)

residual wavefront errors equal to $\phi_{RMS} = 0.053$ waves (Equation 9) or SR = 90%. For estimating the required sensitivity for wavefront sensing, a position accuracy of 10% RMS of the Hartmann-Shack sensor image sizes (λ/r_o) appears reasonable. This results in additional residual wavefront errors of ≈ 0.035 waves RMS reducing the Strehl Ratio to 85%. For photoelectron noise limited detectors (e.g. intensified detectors or very low read-out noise CCD arrays) this means the detection of ≈ 100 photon events per detection time τ_{det}. For detector noise limited applications (infrared detectors and many CCD arrays) it means the detection of $10 \times$ the detector quantum noise per detection time τ_{det}. Until now photon detectors using intensifiers have been preferred, but with the arrival of very low read-out noise ($< 5\,e^-$) CCDs with $\approx 5 \times$ the quantum efficiency of photocathodes, CCD arrays are becoming very attractive (Geary 1992, Wittman et al 1992). Array mosaics and/or arrays with multiple read-out amplifiers are necessary because of the high read-out rates involved ($\tau_{det} \approx 0.3\tau_o \approx 0.004$ sec at visible wavelengths).

Table 3 lists the limiting magnitudes for wavefront sensing for such a visible light wavefront sensor used in the polychromatic wavefront sensing

mode (see Section 4.4) for the different photometric bands, and the resulting sky coverage taking into account the star numbers and the size of the isoplanatic patch (θ_o). Using natural stars for wavefront sensing therefore results in very little sky coverage at visible wavelengths. The sky coverage increases rapidly towards the infrared which is, together with the decreased complexity and cost, the reason why most current efforts focus on the 1–5 μm wavelength region. Sky coverage increases rapidly with improved seeing (approximately proportional to r_o^5 for low sky coverage). Sky coverage also increases towards the galactic equator. Because of the rapid increase in star numbers in the K band, due to the decrease of intra-galactic absorption, it has been suggested to use Hartmann-Shack wavefront sensors in the K band in order to increase the sky coverage (Beckers & Goad 1987, 1988). Rigaut et al (1992a) have carried out the first astronomical experiment with such a near-infrared wavefront sensor. Near-infrared wavefront sensors are presently limited in their sensitivity by the high read-out noise of the detectors. The rapid improvement of the detectors are likely to make near-infrared Hartmann-Shack wavefront sensors of interest in the future. However, only with the introduction of laser guide stars (see Section 9) in astronomical adaptive optics will it be possible to reach almost full sky coverage at all wavelengths. Angel (1992) suggests combining wavefront sensing using both natural and laser guide stars, measuring the low spatial scale aberrations with the natural stars. For these

Table 3 Limiting V magnitude for polychromatic wavefront sensing and sky coverage at average Galactic latitude for different spectral bands[a]

Spectral band	λ (μm)	r_o (cm)	τ_o (sec)	τ_{det} (sec)	V_{lim}	θ_o (arcsec)	Sky coverage (%)
U	0.365	9.0	.009	.0027	7.4	1.2	1.8 E-5
B	0.44	11.4	.011	.0034	8.2	1.5	6.1 E-5
V	0.55	14.9	.015	.0045	9.0	1.9	2.6 E-4
R	0.70	20.0	.020	.0060	10.0	2.6	0.0013
I	0.90	27.0	.027	.0081	11.0	3.5	0.006
J	1.25	40	.040	.0120	12.2	5.1	0.046
H	1.62	55	.055	.0164	13.3	7.0	0.22
K	2.2	79	.079	.024	14.4	10.1	1.32
L	3.4	133	.133	.040	16.2	17.0	14.5
M	5.0	210	.21	.063	17.7	27.0	71
N	10	500	.50	.150	20.4	64	100

[a] Conditions are: 0.75 arcsec seeing at 0.5 μm; $\tau_{det} = 0.3 \tau_o = 0.3 r/V_{wind}$; $V_{wind} = 10$ m/sec; $H = 5000$ meters; photon detection efficiency (includes transmission and QE) = 20%; spectral bandwidth = 300 nm; SNR = 100 per Hartmann-Shack image; detector noise = 5 e⁻.

spatial scales the sky coverage is appreciably larger than those shown in Table 3.

4.2   Wavefront Curvature Measurements

Figure 4 (*left*) shows a long exposure out-of-focus image of one of the six 180 cm mirrors of the MMT. The striking intensity pattern in the image can be interpreted in terms of wavefront curvature variations resulting from the telescope optics as explained in terms of simple geometrical optics by Beckers & Williams (1979). Figure 4 (*right*) depicts the one-dimensional case. Looking at an on-axis star, the ray coming from a point on the pupil P at a distance x from the axis will intersect the out-of-focus plane Q at a distance ξ from the axis. For perfect optics $\xi(x) = x \cdot (F/z)$, where F is the telescope focal length and z is the distance from focus. When the mirror surface is distorted by $\Omega(x)$ this ray will depart from the perfect optics case by an angle $\delta(x) = 2d\Omega(x)/dx$, and its intersection with Q will be $\xi(x) \approx x \cdot (z/F) + \delta(x) \cdot (F+z)$ (approximation valid for small angles). The intensity in the out-of-focus image is proportional to $|d\xi(x)/dx|$ which equals $|(z/F) + (F+z) \cdot d\delta(x)/dx|$, and which shows spatial intensity variations proportional to $d\delta(x)/dx$ or $d^2\Omega(x)/dx^2$, corresponding to the wavefront curvature. These intensity variations are opposite on opposite sides of the telescope focus as also observed by Beckers & Williams (1979). Diffraction effects modify this simple geometric optics derivation, especially for small z where their scale dominates those of the geometrical optics. It is therefore necessary to go quite far outside focus (large z values).

Roddier (1988b, 1990, 1991) has elaborated this concept for wavefront curvature sensing and has applied it, in combination with a variable curvature adaptive mirror (Forbes 1989, Forbes & N. Roddier 1991), to the adaptive optics system being developed at the University of Hawaii
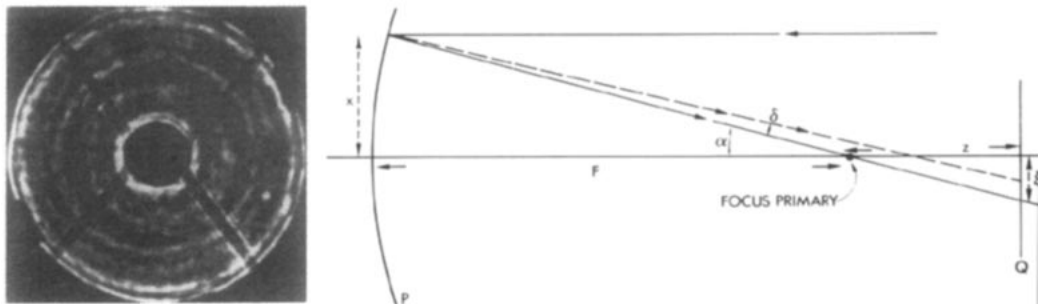

Figure 4   (*Left*) Out-of-focus star image taken with one of the MMT telescopes. (*Right*) Its interpretation using geometrical optics in terms of wavefront curvature (see text).

(Graves & McKenna 1991; N. Roddier 1991; Roddier & Roddier 1988; Roddier et al 1987, 1991a,b). For the short exposure times required for adaptive optics, scintillation effects add to the wavefront curvature intensity effects. Their intensity variations are assumed to be similar on both sides of focus so that the subtraction of the intensity patterns taken at equal but opposite z will to some extent remove them. The out-of-focus intensity patterns of the obstruction caused by the telescope's secondary mirror and its support are, however, quite different and cause complications. The combination of wavefront curvature sensing and control results in substantial advantages in the control of the adaptive optics system since error signal and actuator command are directly coupled. This is not the case for many other adaptive optics systems, where e.g. wavefront tilts have to be converted into wavefront deviations for the control of a continuous surface adaptive mirror. It appears that wavefront curvature assessment competes in sensitivity with wavefront tilt assessment for adaptive optics systems at least for low spatial order adaptive optics systems (Roddier et al 1988).

4.3   Wavefront Estimates Using Neural Networks

Experienced opticians can recognize the dominant types of aberrations from inspection of images, especially when moving in and out of focus. Similarly neural networks can be trained to recognize such aberrations. Interest in such forms of wavefront assessment has recently increased (Angel et al 1990; Sandler et al 1991a,b). Numerical experiments by Sandler et al (1991a) show a fairly good correspondence between the modal wavefront estimates using the neural network and Hartmann-Shack methods for the lower order Zernike modes up to coma (Z_7 & Z_8) for $D/r_o \approx 7$. It remains to be established that this method of wavefront estimation is competitive with other methods, especially at high spatial frequencies. Neural network techniques for wavefront sensing and correction, including telescope co-phasing, have recently been successfully applied to the MMT (Lloyd-Hart et al 1992a,b; Wizinovich et al 1991).

4.4   Polychromatic Wavefront Sensing

The refractive index of air varies little with wavelength for visible and infrared wavelengths. The variation of $(n-1)$ is, for example, less than 2% between the V (0.55 μm) and M (5 μm) bands. As a result wavefront distortions expressed in μm, and hence, for example, the image motions in a Hartmann-Shack sensor, are for all practical purposes identical. This led Woolf & Angel (1980) and Woolf (1984) to propose the concept of *polychromatic adaptive optics* in which the wavefront is measured in one wavelength, but corrected for another. The differential atmospheric refrac-

tion between the different wavelengths will cause the rays to traverse different paths through the atmosphere when looking away from zenith. These differences are, however, small compared to r_o so that they have been ignored. Normally visible wavelengths are used to measure the wavefront for IR applications. The large pupil subaperture, matched to the IR requirements, will cause the visible Hartmann-Shack images to be speckled. Care has to be taken so that this does not increase the noise in the wavefront measurement (Beckers et al 1986).

4.5   Wavefront Amplitude Measurements

Astronomical adaptive optics systems do not yet correct for wavefront amplitude variations since most of the cause of image deterioration is to be found in phase variations (Section 3.1.2). As systems are refined and used at shorter visible wavelength, amplitude variations are likely to become a factor. They are measured simply by imaging the telescope pupil.

4.6   Wavefront Sensors for Incoherent and Extended Objects

The Foucault/knife-edge, Hartmann-Shack and curvature wavefront sensors are all based on geometrical optics and therefore work well on incoherent objects like laser guide stars. Hartmann-Shack sensors, or related modifications, appear to be particularly suitable for extended objects that have surface structure like the large planets or the solar surface with its small sunspots and granulation (Acton 1989; Acton & Smithson 1991, 1992; Smithson et al 1984; Wirth & Ruquist 1985). A liquid crystal device which uses the intensity variations detected when a solar image moves across a previously stored image derivative is being pursued at the Sacramento Peak Observatory (Dunn 1987a, 1990; von der Lühe 1987, 1988, 1991). It works like a multiple knife-edge device on solar surface structure.

5.   THE CORRECTION OF THE WAVEFRONT DISTORTION

5.1   Adaptive Optical Components

With the wavefront distortion known, it is up to the adaptive optical component to correct it. These optical components are mostly mirrors. They have to be designed so that their shape can be adjusted to match the instantaneous wavefront distortion well. They are characterized by: their size, the number of adjustable subareas (or elements), the number of actuators, the wavefront influence function of each actuator, the speed at which they can be adjusted, and their stroke. Since most of the wavefront distortion is in the form of wavefront tilt across the aperture, the function of the adaptive optical component is often divided among two components:

a tip-tilt mirror covering the full aperture and an adaptive mirror which corrects the higher order wavefront distortions. I summarize below the most common adaptive optical components in use. For recent, more detailed, descriptions I refer to Ealey (1991), Ealey & Washeba (1990), Ealey & Wellman (1991), Merkle (1987a), and Tyson (1991).

5.1.1   SEGMENTED MIRRORS   Since most wavefront sensors measure the wavefront tilt over a number of subareas of the telescope aperture, it is advantageous for the control of the wavefront to correct these tilts by an array of mirrors which match those subareas and which individually can directly correct the measured tilts. A number of systems therefore use segmented mirrors (Dunn 1987a, 1989, 1990; Smithson 1987; Smithson et al 1984, 1988). In each segment both piston and tip/tilt are normally adjusted. Segmented mirrors can be made modular. The largest number of segments available so far are 512, but adaptive mirrors of this type with more than 10,000 elements appear feasible (Hulburd 1989, Hulburd & Sandler 1990). Although the tip/tilt of these mirrors can be directly controlled from the wavefront sensor, the piston of the segments can not. In order to assure overall continuity of the surface it is necessary to control it separately. The gaps between the segments are of concern because of light loss, extra infrared thermal emission, and diffraction of light. The former two effects are of little concern for solar applications, which is why segmented mirrors have been used in those cases. Nighttime applications, and recently also solar applications (Dunn et al 1991), mostly use continuous faceplate adaptive mirrors.

5.1.2   CONTINUOUS FACEPLATE MIRRORS   Apart from the advantages indicated above, continuous faceplate adaptive mirrors automatically maintain continuity and therefore can work with a reduced number of actuators. Actuators are generally of the push-pull type using mostly piezoelectric or electrostrictive materials. It is very important that the actuators have influence functions that "mesh" well, thus resulting in a wavefront correction shape that matches the desired correction profile in an optimal way. This is achieved by optimizing the mechanical design of the mirror itself as well as its coupling to the actuators.

Occasionally bending moment actuators are used. Rather than resulting in wavefront displacement reactions their actuators introduce wavefront curvature reactions. The University of Hawaii system (Roddier et al 1991a,b) uses this type of adaptive mirror for its curvature sensing/control adaptive optics system. The curvature actuation is done by bimorph techniques using oppositely polarized piezoelectric materials (Forbes 1989; Jagourel et al 1990a,b; Kokorovski 1979; Steinhaus & Lipson 1979). Bimorph actuators have the same advantage as segmented mirrors with

regard to their capability of using direct wavefront signal–actuator command control, but without the need to control an additional variable (the piston in the segmented mirror). Edge actuators may be used in addition to the bimorph actuation to control lower order aberrations. Roddier (1992a) strongly advocates the use of curvature adaptive optics for the correction of the lower order aberrations on the basis of its economy, of its simplicity of control, and because its influence function which is global across the entire mirror has a spatial behavior similar to that of the Kolmogorov-based atmospheric wavefront structure.

5.1.3   OTHER TYPES   A number of other ways exist in which the optical path across an aperture can be varied. There is the original suggestion for an adaptive mirror using an electron beam scanner on a film of oil as actuator (the Eidophor, see Figure 1) by Babcock (1953, 1958) which to my knowledge has never been pursued. Membrane mirrors use deformation of a thin membrane by electrostatic forces (Clampin et al 1991, Durrance & Clampin 1989, Grosso & Yellin 1977, Merkle et al 1982); they tend to be rather fragile and are used to control lower order aberrations. Liquid crystal technology is also being explored as a way to correct the wavefront (Bonaccini et al 1990, 1991).

5.2   Control of the Adaptive Optical Component

The servo systems which couple the wavefront signal with the actuators of the adaptive mirrors are quite complex (see e.g. Boyer & Gaffard 1991, Boyer et al 1990a,b). Except for the simplest, low order systems, they tend to involve a large number of signals which are to be mixed in the appropriate way to arrive at the commands to be directed to the many actuators. The signals are generally very noisy due to photon or detector noise and care has to be taken to reduce the influence of this noise on the wavefront correction. All of this has to be carried out at high speeds, faster than the time scale τ_o of atmospheric wavefront changes (Section 3.3). The control of adaptive optics systems can therefore be quite complex, sometimes involving analog systems to achieve the high speeds required, but more and more using fast digital controllers since these have the ability to adjust the delicate control algorithms for varying conditions, like flux, noise, r_o, and τ_o changes. Control appears simplest when there is a one-to-one correspondence between each sensor signal and each actuator—as is the case for segmented tip-tilt mirrors and wavefront curvature systems. Such simple direct control requires, however, good, low-noise signals. When this is not so, as is the case with most natural guide stars, the optimum control will require appropriate spatial filtering of the signals and distributed amplitude control on the different scales of the adaptive optical component.

5.2.1   MODAL VS ZONAL CONTROL   In modal control the wavefront signal is expressed by a linear combination of modes, mostly of the Zernike type (Table 2), but also of other types like the Karhünen-Loève functions (see e.g. Wang & Markey 1978) or modes that correspond to the eigenmodes of the particular adaptive optics component used. The control signals to the adaptive optical component are calibrated and combined in such a way as to result in a wavefront distortion of the same form as these modes, and the control loop is closed. The actuator patterns of some adaptive mirrors are optimized for such modal patterns. The time constants can be adjusted easily to give a relatively slow control of the low order and a fast control of the high order aberrations. Modal control is the preferred way to control adaptive optics, at least for the lower order modes. For higher order modes it is still preferred by some. In other systems, however, zonal (also called "nodal") control is preferred. In zonal control no modal expansion is done. Each zone/segment/mirror element is controlled independently by wavefront signals which are also treated individually. The two may be coupled, for example, by means of a control matrix, also referred to as the "reconstructor," approximately the inverse of an influence matrix, which couples the tilt signals to the adaptive optical component distortion. There is an ongoing discussion as to the relative merits of modal versus zonal control for higher order adaptive optics correction.

5.2.2   MATCHING THE COMPONENT TO THE WAVEFRONT SHAPE   The criterion that most control systems try to meet is the optimization of the Strehl Ratio SR. Since for small residual wavefronts the Strehl Ratio deviates from 100% by the variance (RMS^2) of the wavefront residuals Δ (in rad^2, see Equation 10), control algorithms tend to use least squares (LS) fitting techniques to fit the optical component shape to the wavefront signal pattern. LS techniques, while perfect for the control of adaptive optics where the residual wavefronts are small (SR > 50%), are not optimum for so-called partial adaptive optics in which the use of adaptive optics very much improves the image but not enough to bring it close to the telescope diffraction limit.

5.2.3   PARTIAL ADAPTIVE OPTICS   Partial adaptive optics is likely to play a major role in optical astronomy since it will not always be possible to build an adaptive optics system in which the residual wavefront errors are a small fraction of a wavelength. All the systems now being developed for high Strehl Ratio application in the infrared at ≈ 2.2 μm have an element/zone size r_E equal to about r_o (or $r_E/r_o \approx 1$) at that wavelength. They will work in the partial adaptive optics mode at visible wavelengths where the wavefront residual will be ≈ 0.3 waves RMS at 0.55 μm and $r_E/r_o \approx 5.3$, outside the range for which LS fits are optimum. Depending

on the wavefront fitting algorithms used, the partial adaptive optics point-spread-function will assume different shapes ranging from a narrowing of the gaussian-like shape of the seeing profile (Nisenson & Barakat 1987) to that of a spiked helmet-shaped profile in which an Airy-shaped spike is superposed on a broad halo-like background with a width approximately equal to that of the original seeing disk (Peri et al 1988; Smithson & Peri 1987, 1989; Smithson et al 1988; see also Figure 5). It is now clear that for $r_E/r_o < 5$, a LS fitting technique results in a spiked profile with the fraction Σ of the point-spread-function energy in the spike depending on r_E/r_o. This was recently confirmed experimentally (Rigaut et al 1992d). Various estimates of Σ until 1990 were summarized by Beckers (1990). Additional calculations (Beckers 1992a,c; Conan et al 1992; Roggemann 1991; Rousset et al 1992a; Wang & Markey 1978) now give typical Σ values of 75%, 41%, 15%, 9%, and 4% for $r_E/r_o = 1, 2, 3, 4,$ and 5 respectively. Parallel to the point-spread-function shape the modulation transfer function (MTF) of a partial adaptive optics system consists of a mixture of the MTF of a diffraction-limited telescope with amplitude Σ and the MTF of the seeing disk with amplitude $1 - \Sigma$. Rousset et al (1992a) show that these values of Σ rapidly decrease when the adaptive optics time constant is inadequate or when the wavefront sensor signal is very noisy.

A substantial improvement in Σ for $r_E/r_o > 3$ can be obtained by optimizing the fitting algorithm. Beckers (1992a,c) suggested using the so-called maximum fraction (MF) algorithm in which the fraction of the telescope pupil where the residual wavefront distortions are small (e.g.
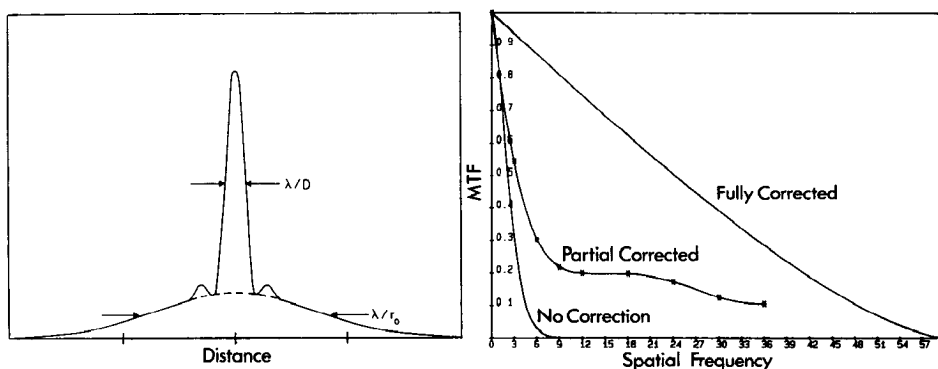

Figure 5   (Left) Schematic point-spread-function of a partial adaptive optics system (from Beckers & Goad 1987). (Right) Modulation Transfer Function for an uncorrected, partially corrected, and fully corrected adaptive optics telescope (adapted from Gaffard & Boyer 1987).

$< \lambda/8)$ is optimized. In contrast to the LS algorithm , the MF algorithm does not try to preferentially reduce the amplitudes of the large residual wavefront excursions. By maximizing the fractional area the central intensity of the point-spread-function is maximized. Using the MF algorithm it is possible to more than double Σ for $r_E/r_o \geqslant 4$ over that achieved by the LS fitting algorithm.

6.   PREDICTED AND ACHIEVED PERFORMANCE

6.1   *Astronomical Performance Criteria*

The usual criterion for the performance of adaptive optics systems has been the Strehl Ratio. For directed energy requirements this is the item of primary interest. It also satisfies most astronomical requirements if a Strehl Ratio close to 100% can be achieved. Depending on the application and on the desired performance of the adaptive optics system one could use different criteria. Roddier et al (1991b) thus prefer to use the "Normalized Strehl Resolution" R/R_{max} (see Section 3.1.3) and "Strehl Width." The latter is defined as the diameter of a uniformly illuminated disk with the same central intensity and same total energy as the point-spread-function.

There are a number of examples of specific astronomy related performance criteria. (*a*) For many *spectroscopic applications* one is primarily interested in the one-dimensional Strehl Width in the direction at right angles to the slit. Disregarding the requirement for a narrow image profile in the direction along the slit may result in an improved limiting magnitude for the guide star. (*b*) The study of stellar *envelopes* would often benefit from the minimization of the halo surrounding a long exposure image even if that occurs at the expense of the energy in the image core. (*c*) For *interferometric imaging* the maximum Strehl Ratio is indeed the optimum (Beckers 1990). (*d*) The study of a *faint companion* in the vicinity of a bright star with a known location would benefit from the minimization of the point-spread-function of the bright star at that position while maintaining the highest possible Strehl Ratio but ignoring the rest of the point-spread-function. I am not aware of studies aimed at optimizing these astronomy related criteria. They suggest, however, another direction for the use of adaptive optics in which it is used to not only flatten the wavefront but also to manipulate it to the maximum extent possible to achieve any desired point-spread-function. Such wavefront manipulation could also include full complex amplitude control, including transmission variations across the pupil (resulting also in the option of apodization control). For the following the usual performance criterion will be taken: the maximization of the Strehl Ratio.

6.2   Causes for Performance Decrease

I summarize below the factors that contribute to determining the performance of a system at its "design wavelength" $(r_E/r_o(\lambda) \approx 1)$. The expressions given here for natural guide stars are approximate. Actual performance has to be derived for each system by modeling and experimentation (see e.g. Gaffard 1991, Gaffard & Delanois 1991, Gaffard & Boyer 1987, Northcott 1991, Roddier & Roddier 1989). The partial adaptive optics case (Section 5.2.3) is much less explored and tends to be more complex.

6.2.1   FINITE SPATIAL RESOLUTION   The finite spatial resolution of both wavefront sensor and adaptive mirror for a zonal adaptive optics system according to Greenwood (1979) and Parenti (1992a,b) lead to residual wavefront variance Δ of:

$$\Delta_{\text{spatial}} \approx 0.34(r_E/r_o)^{5/3}\,\text{rad}^2. \tag{16}$$

This variance is often referred to as the *wavefront fitting error*.

6.2.2   FINITE TEMPORAL RESOLUTION   The assessment of the effect of finite temporal resolution on the performance depends on the servo characteristics of the system. Following Greenwood (1977) one has:

$$\Delta_{\text{temporal}} \approx (f_G/f_{\text{servo}})^{5/3}\,\text{rad}^2, \tag{17}$$

where f_{servo} is the closed-loop servo bandwidth at -3dB of the adaptive optics control system. This servo bandwidth f_{servo} equals approximately $0.3/\tau_d$, where τ_d is the "dwell time" of the adaptive optics system defined as the time lag between the wavefront measurement and its correction (Parenti 1992a,b). This variance is often referred to as the *time delay error* or *servo error*.

6.2.3   PHOTON NOISE   As discussed in Section 4.1.3 one would like for wavefront sensing to have a signal-to-noise ratio (SNR) of at least 10 per subaperture (size r_E) in the Hartmann-Shack tilt measurements, or $N_{\text{pe}} = 100$ photon events in a detector which is photon noise limited. In general one has

$$\Delta_{\text{photon}} = 4 \cdot \text{SNR}^{-2}\,\text{rad}^2 \approx 4/N_{\text{pe}}\,\text{rad}^2. \tag{18}$$

When only a few ($\ll 100$) photons are available the photon noise becomes a severe performance limitation. In that case one corrects only the low order wavefront modes and works in the partial adaptive optics mode (Section 5.2.3).

6.2.4   DEVIATIONS DUE TO POLYCHROMATIC APPROACH   Wavefront devi-

ations due to wavelength variation of the air refractive index are usually ignored in polychromatic adaptive optics (see Section 4.4). To a large extent they can be compensated for in the control system, if needed e.g. at blue and ultraviolet wavelengths, since the wavelength variation is very well known. Hogge & Butts (1982) examined the effects of nongeometrical optics on the wavefront sensing and found significant effects if long wavelengths are used for wavefront sensing and correction is made for shorter wavelengths. This is normally not the case in astronomical adaptive optics. For a wavefront sensing wavelength of 500 nm and a correction at 5 μm they find 0.006 rad^2 at zenith (and 5 μm) which for all practical purposes can be ignored.

6.2.5 DEVIATIONS FROM ISOPLANATISM Already discussed in Section 3.2.2, the Strehl Ratio decreases to about 40% for large D/r_o at offset angles α equal to the isoplanatic angle θ_o.

6.2.6 AMPLITUDE VARIATIONS Amplitude variations are normally ignored even though they may lead to a Strehl Ratio reduction of 10 to 15% at visible wavelengths (Section 3.1.2).

6.3 Predicted and Achieved Performance

The best analyzed astronomical adaptive optics system is the ESO-France COME-ON system as tested on the ESO La Silla 3.6 meter telescope. Table 4 compares the results reported by Rigaut et al (1991) with the predictions based on the estimates given above. The predictions are highly dependant on the value assumed for r_o, r_E, and especially V_{wind} since the time response of the COME-ON system was limited. The predictions for $V_{wind} \approx 25$/sec correspond well with the observations. I refer to Rigaut et al (1991) for a more detailed analysis of the observations. They find that the average wind velocity that best fits the observations is ≈ 15 to 20 m/sec, in reasonably good agreement with the results in Table 4 considering the uncertainties in the modeling of such an atmosphere/adaptive-optics system. Recently the servo bandwidth of the COME-ON system was increased by a factor 2.7 resulting in a substantially improved performance since the temporal values are reduced by a factor of ≈ 5 (Rigaut et al 1992d). The Strehl Ratio decrease due to amplitude effects amount to 4, 3, and 2% for the H, K, and L bands (Roddier & Roddier 1986) and therefore do not affect these conclusions. The predictions and observations in Table 4 were done with a bright guide star, so that photon noise can also be ignored. Rigaut et al (1992a) confirmed the predictions of the effects of a limited SNR in visible light and infrared wavefront sensors. A number of predictions of the performance of adaptive optics systems for

Table 4 Comparison of predicted and observed Strehl Ratios (SR) for the ESO-France COME-ON 19 element adaptive optics system on the La Silla 3.6 meter telescope for three wind velocities $(V_{wind})^a$

Spectral band	Units	J	H	K	L	M
Wavelength	μm	1.2	1.68	2.23	3.87	4.75
r_o (0.5 μm)*	cm	11.5	11.5	11.5	11.5	11.5
r_o	cm	33	49	69	134	171
r_E	cm	100	100	100	100	100
V_{wind}	m/sec	5/15/25	5/15/25	5/15/25	5/15/25	5/15/25
τ_o	msec	21/7/4	31/10/6	43/14/9	84/28/17	107/36/21
f_G	Hz	6/19/32	4/13/22	3/9/15	2/5/8	1/4/6
$\tau_d{}^*$	msec	17	17	17	17	17
$f_{servo}{}^*$	Hz	20	20	20	20	20
$\Delta_{spatial}$	rad^2	2.16	1.12	0.63	0.21	0.14
$\Delta_{temporal}$	rad^2	.15/.95/2.22	.08/.49/1.15	.04/.28/.65	.01/.09/.22	.01/.06/.14
Δ_{TOTAL}	rad^2	2.3 /3.1 /4.4	1.20/1.61/2.3	.67/.94/1.28	.22/.30/.43	.15/.20/.28
$SR_{predicted}$	%	10/4/1	30/20/10	51/39/28	80/74/65	86/82/76
$SR_{observed}$	%	-	10	28	70	-

[a] Values obtained directly from Rigaut et al (1991), Boyer et al (1990a,b), and Gaffard & Boyer (1990) are indicated by asterisks (*). Predicted Strehl Ratios use SR = exp($-\Delta$) relation (Equation 10).

8 to 10 meter astronomical telescopes are now being made (e.g. Ellerbroek 1992a,b; Parenti 1992a,b).

## 7.   FIRST ASTRONOMICAL RESULTS

Most of the astronomical adaptive optics systems listed in Table 1 are still in development or in the planning stages. Two of the systems have recently (August 1992) produced publishable astronomical results. Both have adaptive mirrors with 19 elements; one is used for infrared (2 to 5 μm) nighttime astronomy with large aperture telescopes (1.5 and 3.6 meters);

the other is used for solar observations at visible wavelengths with a modest size aperture (63.5 cm). In addition Golinowski et al (1992) reported first observations of the circumstellar disk of βPic using the Johns Hopkins University Adaptive Optics Coronograph (AOC) using tilt correction only. A number of other higher-order systems (U. of Hawaii, Mt Wilson 60″/ACE, Lincoln Lab SWAT, Phillips Lab SOR) have demonstrated successful image sharpening on bright single and binary stars and are in a position to produce astronomical results shortly.

7.1   The ESO/France Adaptive Optics System (COME-ON)

The COME-ON system was initially commissioned and tested at the 1.52 meter telescope of the Observatoire de Haute-Provence (Merkle et al 1989, 1990a,b,c) where it also produced its first astronomical results (Kern et al 1990a). It then was installed at the 3.6 meter ESO telescope at La Silla where a number of observing campaigns have produced diffraction-limited images of various astronomical objects (Rigaut et al 1992b,c). Preliminary results have been published on the rotation axis of the asteroid Ceres (Saint-Pé et al 1992, Merkle et al 1991b), on the massive star η Carinae (Rigaut & Gehring 1992), on the structure surrounding the young stellar object Z CMa (Malbet et al 1991, 1992), on the Seyfert galaxy NGC 1068 (Rigaut et al 1992c), and on the orbits of close binary systems, especially those that may include brown dwarfs (Mariotti & Perrier 1991, Mariotti et al 1992; see Figure 6).

The COME-ON system is now being upgraded to a 52-element system
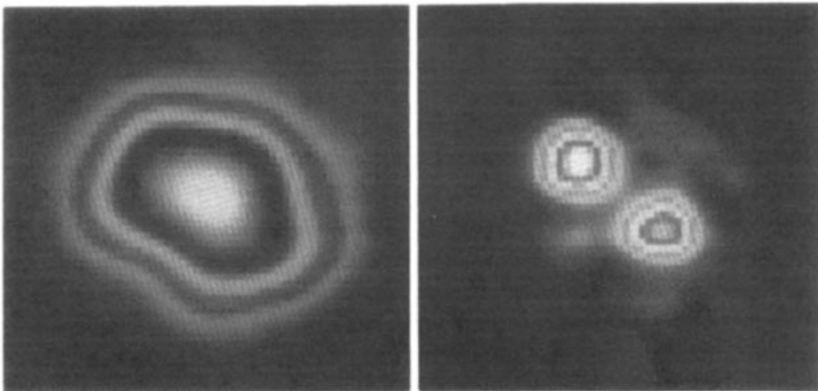
Figure 6   L Band image of the binary star HR 6658 obtained with the COME-ON adaptive optics system on the ESO La Silla 3.6 meter telescope. (*Left*) The uncorrected image (seeing FWHM 0.8 arcsec). (*Right*) The corrected image (FWHM 0.22 arcsec). The separation of the binary components amounts to 0.38 arcsec. (From Merkle 1991.)

(Rousset et al 1992b) to be used at the ESO La Silla 3.6 meter telescope. It will have a 3 dB closed-loop servo bandwidth of ≈ 65 Hz (vs only 20 Hz for the original COME-ON system) and will further be optimized with a control system that adjusts itself to the variable observing conditions (a kind of artificial intelligence). The intention is to make it "user-friendly" to serve a broad community. This COME-ON-PLUS system will also serve as a true-scaled engineering and operational prototype for the 256-element adaptive optics system which will be part of each of the 8 meter VLT telescopes.

7.2   Lockheed/SPO Solar Adaptive Optics System

Figure 7 shows an image of a small sunspot and its surrounding area obtained with the Lockheed/SPO adaptive optics system at 520 nm wavelength (Acton & Smithson 1992). Wavefront sensing was done with a Hartmann-Shack–like device using the small sunspot (pore) in the image. Observations away from solar active regions will require the development of wavefront sensors using quiet solar surface structures such as solar granulation.
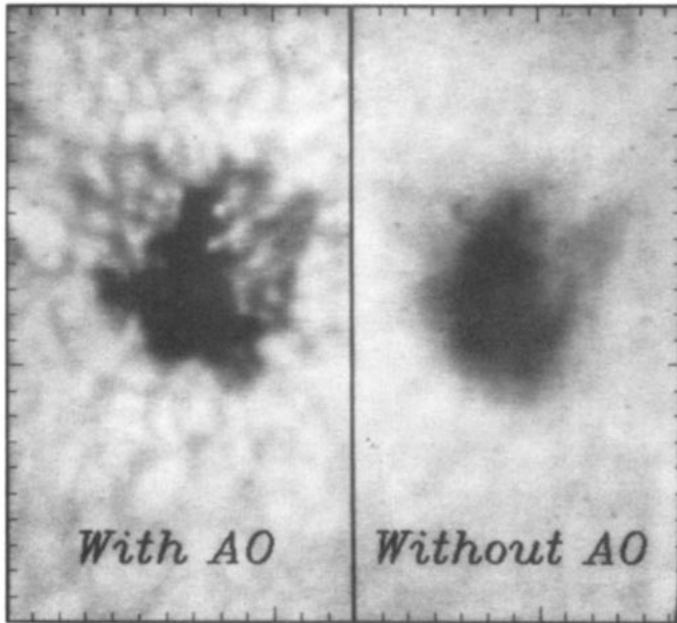

Figure 7   Image of a small sunspot on the solar surface obtained with the Lockheed/SPO adaptive optics system at 520 nm wavelength with a telescope aperture of 32 cm. (*Right*) Uncorrected image. (*Left*) Corrected image. The divisions at the edge of the image are 1 arcsec apart. (From Acton & Smithson 1992.)

8.   ASTRONOMICAL APPLICATIONS OF ADAPTIVE OPTICS SYSTEMS AND THEIR LIMITATIONS

8.1   *Applications of Adaptive Optics to Astronomy*

There is a wide diversity of possible applications of adaptive optics in astronomy. I describe some of them in this chapter, focusing more on classes associated with this diversity than on a complete overview of all applications.

8.1.1   IMAGING   The most obvious applications of adaptive optics relate to the direct broad and narrow band imaging (and spectroscopy) of such extended objects as the sun, planets, other solar system objects, giant and supergiant stars, stellar envelopes (including objects like βPic), young stellar objects, and star forming regions. The 1/20 arcsec direct resolution in the K band, and eventually the 1/100 arcsec resolution at visible wavelengths obtainable with 8 to 10 meter telescopes will allow the observations of physical conditions on scales hitherto unachievable or achievable only with the much less sensitive speckle imaging techniques. The same is true for solar observations with 1/25 arcsec, or 30 km solar surface resolution, which will be achieved by the use of visible light adaptive optics on the 240 cm diameter LEST solar telescope. Often the object itself, or its central star, will be bright enough for wavefront sensing. For this application the most appropriate requirement for wavefront control will be the optimization of the Strehl Ratio (or of the fraction Σ of the energy in the central, Airy-shaped spike) and of the system modulation transfer function.

8.1.2   RESOLVING COMPLEX CONFIGURATIONS   The spiked point-spread-function will allow astronomers to resolve many complex configurations in which the sheer number of stars and other objects had previously inhibited observations before. These may be objects such as the central regions of globular clusters, the central region of our Galaxy, and a variety of components in other galaxies. Wavefront sensing may be possible on configurations of stars near the central regions of such nearby globular clusters as 47Tuc and ωCen for full adaptive optics in the K or L band, although it is likely that this application will have to wait for the availability of laser guide stars. The presence of the bright infrared source IRS7 within 6 arcsec of the center of our Milky Way provides a unique opportunity for wavefront sensing which would allow imaging of the complex region near the Galactic Center. In other galaxies, bright stars (like Cepheids) can become resolved in the spiral arms and structure in the cores made visible. Except for using the cores of some bright Seyfert galaxies,

wavefront sensing for most extra-galactic objects will only be possible if a bright foreground star is available. The general examination of galaxies will have to wait for laser guide stars (Section 9). High redshift galaxies ($z > 0.1$) are, however, very numerous so that even though the sky coverage using natural guide stars is very small (see Table 3), many galaxies and QSOs can be studied at near-infrared wavelengths (Beckers 1987b, see also Table 5). Laser guide star technology is therefore not needed in these cases, except for visible wavelength adaptive optics where decreased sky coverage and scattered light effects conspire to decrease the numbers to zero.

8.1.3   DETECTION OF FAINT POINT SOURCES   Going from seeing- to diffraction-limited observations will very much improve the detectability of faint point sources against the sky background. The contrast will increase by $SR \cdot D^2/r_0^2$. One might expect to see many more QSOs as well as many other unknown objects. For full adaptive optics working in the K band

Table 5   Estimates of number of high redshift galaxies and QSOs which can be observed in the vicinity of natural guide stars (NGS)[a]

Wavelength	0.44 μm (B)	0.90 μm (I)	2.2 μm (K)	5.0 μm (M)
Limiting V Magnitude NGS	8	11	14	17
Radius Isoplanatic Patch (θ_o)	1.5"	3.5"	10"	27"
Sky Coverage (Galactic Pole)	3×10^{-7}	2×10^{-5}	4×10^{-3}	2×10^{-1}
Nr. Galaxies at z = 0.4 covered (10^4/□°/mag)	1×10^2	1×10^4	2×10^6	1×10^8
Galaxy Brightness at z = 0.4	23.3		18.5	
"Scattered" Light from NGS (m_V/□" at θ_o/2)	10	15	23	31
Sky Background (full/new moon) (mag/□")	22/17		13/13	
Nr. QSO's covered (total 10^4)	0	0	40	240
"Scattered" Light from NGS (m_V/8^m diffraction disk at θ_o/2)	20 ?	23	29	35

[a] "Scattered" light estimates from observed aureola observations (King 1971, Woolf 1982). Conditions as in Table 3.

(SR = 80%) the relative brightness with respect to the sky background will increase more than a hundredfold for an 8 meter telescope and good seeing (0.8 arcsec). At visible wavelengths the increase will be even larger ($\approx 400\times$) even for an adaptive optics system built for the near-infrared since the decrease in the Strehl Ratio and Σ (both $\approx 10\%$) for the partial adaptive optics are more than offset by the decrease in the area of the diffraction disk.

8.1.4 OBSERVATION OF FAINT COMPANIONS   Like the sun and its solar system, most stars have "stellar systems." Stellar companions can be bright objects observable by direct imaging, by speckle and multi-aperture interferometry, or by spectroscopic techniques. Faint companions ($\Delta m > 7$) are, however, difficult to observe unless well separated from the primary object. Observations of the white dwarf Sirius B with $\Delta m_V = 10$ at a distance of 11 arcsec from Sirius A have amply demonstrated the difficulties. The faint object is hard to observe because of a combination of the light present in the aureola of the bright object and because of diffraction on the spiders supporting the secondary mirror of telescopes. Roddier (1981) and Woolf (1982) showed that the inner (out to ≈ 10 arcsec) aureola brightness as described by King (1971) corresponds very closely to that predicted by atmospheric seeing theory based on Kolmogorov turbulence. Adaptive optics will therefore improve the detection of faint objects in two ways: (a) by decreasing the image size, the contrast, with respect to the bright star aureola and spider diffraction, increases by many magnitudes, and (b) if the adaptive optics has a sufficiently high spatial frequency response, the aureola brightness itself decreases. Combined with the decrease in aureola brightness, care has to be taken to control to the maximum extent possible the effects of spider refraction, possibly by adding amplitude control (in its simplest form: spider masking) to the adaptive optics system. The major contributor to the detectability of faint companions observed with large telescopes appears to be the contrast increase resulting from the decrease in image size. Beyond this, one option might be to manipulate the wavefront to affect a decrease in the diffracted energy at the location of the object without affecting the Strehl Ratio.

8.1.5 CORONOGRAPHY   Coronography aims specifically at decreasing the aureola around bright objects like the sun. It requires low scattered light optics, a point-spread-function with low wing intensities, and the control of the diffraction on spiders and on the boundaries of the optics. The detection of faint point-like companions falls in this class, but coronography specially focuses on the detection of extended objects around the bright star where the large gain due to the contrast increase is less of a

contributor. Examples of such objects are: stellar envelopes and disks including objects like γCas andβPic and QSO surroundings. Adaptive optics designed to decrease the point-spread-function wings would presumably have a different control algorithm than those optimized to maximize the Strehl Ratio. This has to be further explored. One should also examine the utility of full complex amplitude control to achieve the same results. Experiments on coronography using adaptive optics are described by Clampin et al (1991), Durrance & Clampin (1989), and Malbet (1992).

8.1.6   SPECTROSCOPY OF POINT-LIKE OBJECTS   In seeing-limited, large aperture telescopes the best spectral resolution R that can be achieved is coupled in a linear way to the telescope diameter D. This is the result of the limited dimension (d_g) in which gratings can be produced. The designers of high resolution astronomical spectrometers making use of all the tricks in the book (image slicers, pupil slicers, grating mosaics, high diffraction angles, etc) still end up with very large spectrographs located at the Nasmyth or coudé focus which can only achieve resolutions of at best 100,000. The implementation of adaptive optics removes this coupling of spectrograph size with telescope size since the image size decreases proportionally with the telescope diameter increase. It can easily be shown that a slit width corresponding to $2.44\lambda/D$ (the diameter of the first Airy dark ring containing 83% of the energy) results in a spectral resolution R of approximately $0.8 d_g \tan\beta/\lambda$, decreasing inversely with increasing slit width, independent of D and of the focal ratio of the telescope or spectrograph (β = grating blaze angle). In this approximation the beam size diameter on the grating has been taken to be the geometrical one and the diffraction on the edges of the grating or its collimator has been ignored. These are reasonably good approximations for the assumed slit width. For narrower slits the approximation breaks down (R increases to a maximum of $\approx 2 d_g \tan\beta/\lambda$ with substantial light loss due to slit diffraction). For $d_g = 100$ mm, $\tan\beta = 2$ (R2 grating), and $\lambda = 500$ nm, R equals 320,000. A telescope focal ratio of f/15 would make the size of such a spectrograph compact (about 2 meters), which opens the cassegrain focus as a possible location. Its slit width would be 18.3 μm, and with a f/15 camera it would match well to the smaller ≈ 7.5 μm CCD pixels which are available allowing the use of very large format, single chip CCD arrays.

8.1.7   INTEROMETRIC IMAGING   The sensitivity of interferometers increases dramatically ($\Delta m_V > 0.5$) when all electromagnetic radiation is mixed using phased telescope apertures with their corresponding "single speckle," Airy disk shaped images rather than using multi-speckled apertures and images (Merkle 1989a). This is even the case when only partial adaptive optics is used (Beckers 1990, 1991a; Rousset et al 1992a). In some

interferometer applications (e.g. 2 aperture interferometers using pupil plane beam combination) it is sufficient to make the wavefront of the telescopes equal rather than flat. This has led to the concept of "differential adaptive optics" (Beckers 1991b, 1992b).

8.2   Limitations to the Use of Adaptive Optics in Astronomy

Adaptive optics (using natural guide stars) will have some major limitations. Among these are: (*a*) the *sky coverage limitation* already shown in Table 3, (*b*) the limitation to relatively *bright objects*, and (*c*) the *variation of the point-spread-function* with position across the field-of-view (the isoplanatic patch and beyond) which complicates relative photometry and additional image restoration/super-resolution techniques. In this respect adaptive optics may even be at a disadvantage with respect to speckle interferometry techniques where the calibration of the transfer function at different spatial frequencies is better defined and constant across the field-of-view. Finally, (*d*) *light losses* and *increased infrared emissivity* will occur due to the additional optical elements necessary to form the image. Noise, introduced in the thermal infrared background by the varying lightpath in telescopes associated with adaptive optics, proves not to be a significant limitation (Roddier & Eisenhardt 1985, 1986). Recent developments in the implementation of laser guide stars and associated techniques promise to remove most of these limitations.

9.   REMOVING THE LIMITATIONS OF ASTRONOMICAL ADAPTIVE OPTICS

9.1   Full Sky Coverage by Means of Laser Guide Stars

By far the largest limitation to the application of adaptive optics to astronomy is the very limited sky coverage (Table 3) when using natural guide stars for wavefront sensing. Similar limitations existed for many military applications of adaptive optics. Feinlieb (1982) and Happer & MacDonald (1982) suggested a solution in the classified literature to remove this limitation. Independently, Foy & Labeyrie (1985) suggested the same solution in the open literature. The solution uses artificial, laser guide stars for wavefront sensing; these are created by laser light scattering in high layers of the atmosphere. In Feinlieb's proposal Rayleigh scattering in lower layers was suggested. In Happer & MacDonald's and Foy & Labeyrie's proposals scattering off the 90 km high mesospheric neutral sodium layer was proposed. The latter is of most interest for astronomical applications since the resulting laser guide star is located well outside the atmospheric seeing layers and as far away as possible [except for the satellite-borne laser guide stars proposed by Greenaway (1991, 1992)]. Therefore, I

describe only the sodium laser guide star concept in the following; the
Rayleigh laser guide star concept is quite similar.

9.1.1   DESCRIPTION OF THE CONCEPT   The sketch in Figure 8 depicts the
concept of the laser guide stars. A laser tuned to one of the sodium D lines
(normally the D_2 line at 589 nm) is pointed at the ≈ 11.5 km thick layer
of enhanced neutral sodium and potassium located at an altitude of
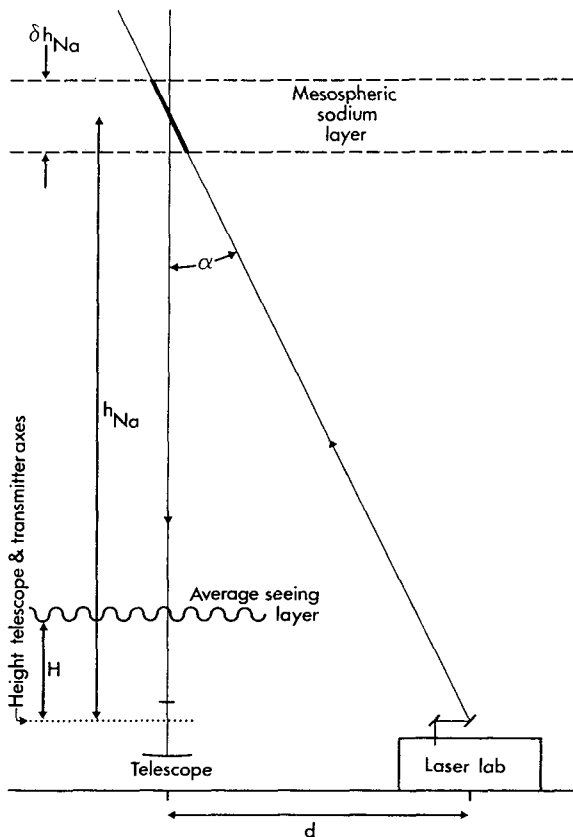approximately 90 km (see e.g. Megie et al 1978). The excess of neutral

Figure 8   Sketch of the telescope—laser transmitter—laser guide star geometry. Plane of
the figure corresponds to the plane containing these three objects. For simplicity it is shown
for a zenith-pointing telescope. Notations: h_{Na} = height of mesospheric sodium layer (≈ 90
km); δh_{Na} = full width at half maximum (FWHM) of sodium layer (≈ 11.5 km); H = average
height of the seeing layer (≈ 4 km); D = telescope diameter (8–10 meter for present gen-
eration telescopes); d = distance of the telescope to the laser transmitter; α = pointing differ-
ence between telescope and laser transmitter. (From Beckers 1992d,e.)

sodium at that layer is thought to originate from meteoric dust. LIDAR observations show a column density of neutral sodium of about 2×10^9 atoms/cm^2 in that layer. The column density, thickness, and height all vary with time. The optical thickness of this layer at the sodium line center equals about 0.05. When illuminated by the laser, sodium atoms are radiatively excited from the $^2S_{1/2}$ ground layer to the $^2P_{3/2}$ layer from which they depart either by a spontaneous emission (in $\approx 10^{-8}$ sec) back to the ground level, emitting photons in all directions, or by stimulated emission to the same level emitting photons in the same direction as the incoming photons. Some of the spontaneously emitted photons return to Earth and reach the telescope to be viewed as the laser guide star. They are used for the sensing of the wavefront. Since the scattering occurs over a range of heights the phases of the returning photons are random. Since Hartmann-Shack and curvature sensors are geometrical optics devices this does not affect the wavefront tilt or curvature sensing. Increasing the energy in the sodium laser beam will increase the intensity of the laser guide star up to the point that the intensity becomes high enough to cause the stimulated emission to dominate the spontaneous photon emission. At that point the laser guide star brightness ceases to increase and "saturation" occurs. For a 50 cm, or $a \approx 1$ arcsec apparent diameter laser guide star, saturation occurs at a laser power of about 5 kW in the pulse. At larger laser guide star sizes the saturation occurs at proportionally higher power levels so that the loss in wavefront sensing sensitivity due to the larger laser guide star spot is offset by the higher laser guide star brightness. For low power lasers this is of course not the case. In any case the laser guide star has to have a diameter $< 2\theta_o$.

9.1.2 STATUS OF LASER GUIDE STAR EXPERIMENTATION   Table 6 summarizes the published capabilities of the demonstrated and planned sodium laser guide stars (see also Kibblewhite 1992a,b). Existing laser guide stars are bright enough for full adaptive optics down to wavelengths of 1 μm. It is expected that laser guide stars as bright as $m_V = 6$ will soon be available (Max et al 1992a,b) allowing their use at visible wavelengths. Laser guide star aided adaptive optics systems have been successfully demonstrated on astronomical objects using Rayleigh scattering laser guide stars for wavefront sensing in 1988 by the MIT Lincoln Laboratory on the 60 cm diameter telescope at AMOS/Haleakala (Primmerman et al 1991) and in 1989/1990 by the USAF Phillips Laboratory on the 150 cm diameter telescope at the Starfire Optical Range/Albuquerque (Fugate 1992b, Fugate et al 1992) following an earlier demonstration of the capability of using Rayleigh laser guide stars for wavefront sensing (Fugate et al 1991). Foy (1992) and Foy et al (1992) summarize the current research

on laser guide stars in France (see also Foy et al 1989). Sodium laser guide stars have so far appeared to have been used for wavefront sensing only (Humphreys et al 1991) but they should soon be used for controlling full adaptive optics systems.

9.1.3   REMOVAL OF THE FOCUS ANISOPLANATISM EFFECT   Three complications arise from the limited distance of the laser guide star from the telescope rather than the effectively infinite distance to the stars: 1. The laser guide star only senses the atmospheric wavefront distortions between it and the telescope and not those of the atmosphere beyond. [This is only a problem for Rayleigh laser guide stars and not for high altitude sodium laser guide stars (see Figure 2).] 2. The laser guide star focuses at a different position than the real star. Since the distance of the laser guide star to the telescope is well known, the resulting defocus signal of the wavefront sensor can be corrected for. 3. The rays from the laser guide star traverses a different airpath from the rays coming from the astronomical object. For a sodium laser guide star located on the telescope axis at a distance from the telescope of h_{Na}, the ray coming from it differs in distance from a ray coming from an on-axis star by $(h/h_{Na})r$, for a distance r from the center of the telescope pupil. For $h_{Na} = 90$ km, $h = 9$ km (the upper troposphere), and r equal to the telescope radius R of say 4 meters, this distance equals 40 cm—which is larger or comparable to the Fried parameter r_o. This effect is referred to as *focus anisoplanatism*. Its effect on the Strehl Ratio has been estimated by Goad (1991) and by Welsh & Gardner (1991). To remove it the use of multiple laser guide stars at slightly different sky locations has been suggested (Foy & Labeyrie 1985). Three to four laser guide stars may suffice. By appropriate combination of the resulting wavefront signals (also referred to as "stitching" of the wavefronts) the wavefront distortions for a star can be derived. First experiments demonstrating this technique have been reported (Murphy et al 1991, 1992).

9.1.4   REMOVAL OF THE TILT DETERMINATION PROBLEM   The upgoing laser beam is affected by atmospheric seeing causing both some blurring and motion of the laser spot on the scattering layer. When observing the laser spot this blurring and motion will be added to the same effects resulting in the air path in the return beam. The blurring/motion effects introduced by the upgoing beam are identical for all Hartmann-Shack sub-apertures and therefore do not affect the differential wavefront tilt measurements except for a decrease in sensitivity due to the blurring. The seeing motion introduced in the upgoing beam will, however, cause a common motion signal in the wavefront sensor which causes it to be different from that of the motion of the star image caused by atmospheric seeing. In the special

Table 6 Published properties of lasers used for laser guide star generation on the mesospheric sodium layer

Authors	Pulse length (μsec)	Rate (Hz)	Duty cycle (%)	Energy per pulse (J)	Average power (W)	Power in pulse (W)	Predicted stellar magnitude[1] (V)
Thompson et al. (1987, 1988, 1989)	2.0	7.5	.0015	.020	0.15	10 000	14
Jeys et al. (1989)	0.1	1000	.01	.0003	0.3	3 000	12
Humphreys et al. (1991)	4.0	20	.008	.12	2.4	30 000	12
Max et al.(1992a,b), Gavel et al.(1992)[2]	0.8	26000	2	.07	≥100	≥5000	≈ 6
Ultimate Limit :			100		5 000+	5 000+	2
ADAPTIVE OPTICS NEEDS (.67" seeing)							I-CCD/CCD[3]
2.20 μm (K)							13/15
1.62 μm (H)							12/14
1.25 μm (J)							11/13
0.90 μm (I)							10/12
0.70 μm (R)							9/11
0.55 μm (V)							8/10
0.44 μm (B)							7/9

[1] Assumes 2×10^9 Na atoms/cm² in the mesospheric sodium layer which is the minimum value. The actual value varies, and can be as much as a factor of 4 larger. The optical depth at line center equals approximately 0.05. Assumed laser guide star image diameter = 1 arcsec or 50 cm at the mesospheric sodium layer.
[2] Planned.
[3] I-CCD = intensified CCD; CCD = bare CCD.

case where the telescope itself is used as the laser transmitter the two laser guide star motions will actually compensate each other causing the laser guide star spot to be stationary (Séchaud et al 1988). This difference between the motion/tilt signal in the wavefront sensor is referred to as the "tilt determination problem." The wavefront tilt (Z_2 and Z_3) must therefore be determined from a stellar signal itself. The chances of finding a bright enough star ($m_V \approx 21.5$ with an 8 meter telescope at V) within θ_o is, however, small (4% for the average sky). The area in the sky for which the image motion is small compared to the width of the diffraction-limited point-spread-function obtained with the laser guide star is $\theta_m \approx 2(D/r_o)^{1/6}\theta_o$ rad in radius for an $\approx 25\%$ Strehl Ratio decrease (Chassat 1989; F. Roddier, JOSA preprint). For an 8 meter telescope and for the conditions listed in Table 3 this implies $\theta_m = 7.5$ arcsec for the V band. Within this area the probability of finding the $m_V = 21.5$ star needed for wavefront tilt sensing is 50% for the average sky (only $\approx 5\%$ at the galactic poles). Rigaut & Gendron (1992a,b) therefore propose the use of dual adaptive optics to overcome the tilt determination problem. In it laser guide star aided adaptive optics is used both on the astronomical object of interest as well as on the star to be used for tilt determination up to θ_m away. With the latter now diffraction limited, this allows the tilt to be determined well enough to allow compensation. Their detailed analysis also shows that this technique results in better than 50% sky coverage for an 8 meter telescope at visible wavelengths for very good seeing ($r_o = 20$ cm). Olivier et al (1992a,b), on the other hand, analyze the case in which single beam adaptive optics is used combined with as good as possible tracking on a nearby star. They find for $D = 10$ meter, $r_o = 13.3$ cm, and 50% sky coverage, the typical residual image motion is 0.026 arcsec RMS as compared to an Airy disk size of 0.011 arcsec at V, resulting in an image broadening of a factor of 3–5 to ≈ 0.045 arcsec. At the cost of a substantial increase of complexity, dual adaptive optics therefore results in substantial improvement. It may also be possible to estimate the wavefront tilt from the laser guide star itself by making it polychromatic. Foy et al (1992) have suggested ways of creating such a polychromatic guide star by, for example, exciting the ${}^4D_{5/2}$ level of the sodium atom by (quasi-)monochromatic laser radiation. The de-excitation of that level then results in a sodium laser guide star which emits in lines at 330, 589, 1140, and 2207 nm. From the differential motions of the guide star at these wavelengths it might then be possible to infer the absolute motion.

9.1.5 REMOVAL OF THE PERSPECTIVE ELONGATION EFFECT   When the laser transmitter is displaced from the telescopes as shown in Figure 8 (also

referred to as the "bistatic" configuration as compared to the "monostatic" configuration where the telescope and the laser transmitter share the same aperture) the laser guide star will appear to be elongated. The amount of elongation depends linearly on the distance d of the transmitter-receiver with $d = 10$ meter resulting in an elongation of ≈ 3 arcsec. This elongation results in a decrease of sensitivity for wavefront sensing even if care is taken to keep the elongation less than the diameter of the isoplanatic patch $(2\theta_o)$. This can be avoided, except for a small effect at the edge of large 8–10 meter diameter astronomical mirrors, by using a monostatic configuration. Bistatic configurations are, however, attractive both because they decouple the transmitter from the telescope, thus simplifying the incorporation of the laser in the system, and because they place the laser Rayleigh and Mie scattering by the Earth's lower atmosphere outside the isoplanatic field of the telescope. Beckers (1992d,e,f) proposes removing this perspective elongation through the use of pulsed lasers of the types given in Table 5. When viewed with μsec time resolution the laser guide star then appears as a round spot which appears to move in ≈ 60 μsec across the 15 km high mesospheric sodium layer. Rapid tracking of this motion in the Hartmann-Shack wavefront sensor by, for example, moving the charges along its CCD detector columns would maintain the sharpness of the laser guide star and hence the laser guide star sensitivity.

9.1.6 INCORPORATION INTO LARGE TELESCOPES AND OBSERVATORIES A number of papers have been published describing the incorporation of laser guide stars in astronomical telescopes and evaluating the resulting expected performance (Ellerbroek 1992a,b; Gavel & Morris 1992; Gardner et al 1989, 1991; Parenti 1992a,b; Parenti & Sasiela 1992; Welsh 1991a,b; Welsh & Gardner 1989, 1991). Most of these papers go into considerable technical detail and I refer to them for those desiring a more detailed description of the methodology of using laser-guide-star-aided adaptive optics for individual large astronomical telescopes.

Because of the limited number of good astronomical sites available, and because of the expenses of developing and operating observatories, astronomical telescopes tend to occur in clusters. Therefore, when incorporating laser guide stars in telescopes one has to consider not only the effect on the properties of the telescope itself but also on all the telescopes at the observatory site. For a telescope using the laser guide star one has the choice of a monostatic or bistatic configuration as discussed above. In a monostatic configuration the laser beam can be transmitted from one of the telescope foci, or from a transmission system mounted on the side(s) of the telescope tube or in front of the secondary mirror. Doing so poses

an interesting challenge to the telescope engineer, especially when retro-fitting it to an already existing telescope. Bistatic configurations avoid this at the expense of putting limits either on the laser pulse length or on the wavefront assessment sensitivity.

As Table 5 shows, the average power and the peak power of the laser transmitter will tend to be rather high especially when laser guide stars for visible light astronomy will be used. Mie scattering on dust and aerosols and Rayleigh scattering on molecules will therefore cause an increase in sky background when looking in a direction which encompasses the laser beam. The amount of average power scattered light is of concern for long duration ($>$laser pulse rate) exposures; a large amount of peak power scattered light will affect high speed photometry. Figure 9 shows the difference $\Delta m_V(h,\varphi)$ in sky brightness between the laser star and the scattered laser radiation to be expected from aerosol and Rayleigh scattering as a function of height h in the atmosphere ($h = 0$ at sea level) and of the angle φ between the outgoing laser beam direction and the telescope viewing direction. It assumes a 1 arcsec^2 size laser guide star, a laser beam diameter of 50 cm, and laser power low enough to avoid significant stimulated emission (peak power $\ll 5$ kW). Figure 9 refers to a small telescope subaperture (< 50 cm) or to naked eye observations. For larger apertures the sky brightness background will be diluted and becomes uneven in the focal plane; its behavior depends on the configuration of the telescope/laser transmitter/viewing directions.

Since for visual light adaptive optics one envisages a $m_V \approx 7$ (see Tables 3 and 6) the sky background due to scattered laser light may amount to one $m_V = 14$ to 18 V star per arcsec^2. This has to be compared with a typical sky background on moonless nights of one $m_V = 21.5$ star per arcsec^2 in all radiations or of one $m_V = 24.5$ star per arcsec^2 in the bright $\lambda 5577$ atmospheric OI emission line. Laser background suppression of a factor of up to $\approx 10^4$ will therefore be necessary. In telescopes that incorporate the laser guide star monostatically the scattered light issues are much worse. It is proposed to control them with fast shutters which only allow star light in the astronomical instrument at the times when the pulsed laser is in the off-stage (Zollars 1992). Additional scattered light reduction is possible by the use of notch filters which block the laser radiation from entering the instrument. Both techniques result in light efficiency loss of the telescope—a loss which will be more than offset by its diffraction-limited performance. Similar techniques can be used for the other telescopes on the site provided all lasers are pulsed simultaneously if the shutter technique is used. Notch filters are, however, likely to be sufficient to eliminate the laser scatter problems.
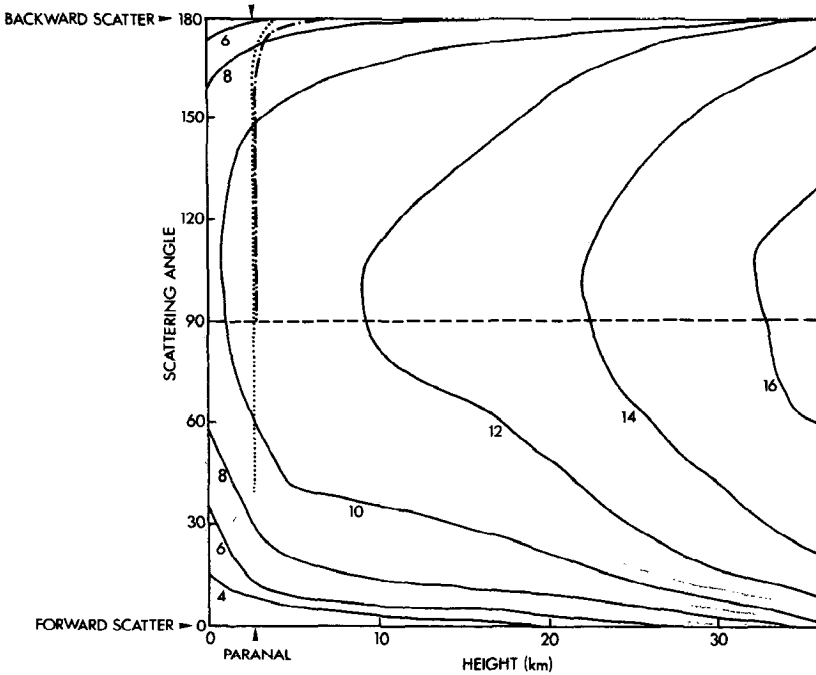
Figure 9   Diagram showing the magnitude difference $\Delta m_V(h,\varphi)$ (per arcsec^2) between the laser guide star and the laser beam scattered light as a function of height h in the atmosphere and scattering angle between the laser and telescope viewing direction. Dashed curve for laser pointing at zenith; dotted curve for laser pointed at 60° zenith distance. Telescope is located 100 meters from laser transmitter, pointed at the laser beam. Scattering from dust particles is not included. Scattering coefficients obtained from *Handbook of Optics*, McGraw-Hill, chap. 14.

9.2   *Increasing the Isoplanatic Patch Size by Multi-Conjugate Adaptive Optics*

There have been a number of proposals to increase the size of the iso-planatic patch by the use of a number of adaptive mirrors placed at the conjugates of different layers of the atmosphere (Beckers 1988a,c, 1989b; Dicke 1982; Foy & Labeyrie 1985; Jankevics & Wirth 1991; Johnston & Welsh 1991; Shamir & Crowe 1992; Tallon & Foy 1990; Tallon et al 1992a,b). The technique requires that one first determine the full 3-D structure of the atmospheric wavefront distortion. This can, in principle, be done by means of "atmospheric tomography," which employs pro-

jections of the wavefront distortions at ground level from arrays of laser guide stars or, in the case of extended objects with surface structure like the sun, by wavefront sensing on different parts of the object. Since much of the seeing occurs near the Earth's surface and at the tropopause, a two-component adaptive optics system with adaptive mirrors located at the conjugates of these layers would already help a great deal (Dicke 1982; Tallon et al 1992a,b). Even a single-component (conventional) adaptive optics system with the adaptive mirror located at the conjugate of the average seeing layer rather than at an image of the pupil (as is usual) would significantly increase the size of the isoplanatic patch. An additional benefit of a multi-conjugate adaptive optics system will be the reduction of the amplitude variations.

9.3 The Integration of Adaptive Optics into the Telescope

At this moment, since adaptive optics systems are still experimental, laser guide stars and adaptive mirrors and their associated optics are generally combined in a package placed like an instrument at one of the focus stations of a telescope. The amount of optics is often quite staggering in order to make the package fit the generally quite limited space and in order to reimage the pupil and image respectively on the tip-tilt mirror and/or the adaptive mirror and on the detector. As a result light is lost, emissivity and scattered light is increased, and the expensive adaptive optics system is available at only one location. In the future as adaptive optics becomes more routine one might expect therefore a better integration in the telescope. The VLT does so partly by including the adaptive mirror in the coudé optics train. It makes adaptive optics available at its coudé focus and its combined coherent and incoherent foci. Beckers (1989a) and J. R. P. Angel (1992, personal communication) suggested making the secondary mirror of the telescope the adaptive mirror. It would feed all foci except the prime focus. By making it ellipsoidal in a Gregorian telescope it could be located at the conjugate of an atmospheric seeing layer. To my knowledge no curved adaptive mirrors exist, but construction techniques used for most of the flat mirrors in existence now could be used for such a mirror. The wavefront sensor would still have to be located at the focus being used, but it and the beamsplitter feeding it would be the only components located there.

10. CONCLUSION

Adaptive optics systems for astronomical telescopes are still in their infancy. Developing them for common use in large telescopes at all wavelengths will take major efforts. It will be expensive—amounting to an

appreciable fraction of the cost of the telescope. Nonetheless it will be exceedingly cost effective in terms of the enhanced capabilities of the telescopes. I expect that the gain in telescope power by making it diffraction limited will exceed that by making it larger. It is unfortunate that the power of telescopes is commonly expressed in terms of its collecting diameter or area and not by its angular resolution. But even the latter depends on the telescope size, so that we may come to think of the power of telescopes in terms of its resolution diameter as well as its collecting diameter.

The field of adaptive optics is in very rapid development. The recent declassification of US military research in this area has resulted in a major leap ahead in its astronomical application. This review represents therefore a snapshot of a rapidly changing, exciting topic. I tried to keep it up-to-date until the latest possible date (August 1992). I gratefully acknowledge the cooperation of my colleagues in the field in keeping me informed of their work. This review is addressed to an astronomy audience and therefore emphasized the astronomical aspects of the topic of adaptive optics at the cost of de-emphasizing the technical aspects. The wide knowledge and experience of technical aspects of adaptive optics obviously warrant a full comprehensive monograph of its own.

Literature Cited

Acton, D. S. 1989. In *High Spatial Resolution Solar Observations*, ed. O. von der Lühe, pp. 71–86. Sunspot, NM: Natl. Sol. Obs.
Acton, D. S., Smithson, R. C. 1991. *Proc. SPIE* 1542: 159–64
Acton, D. S., Smithson, R. C. 1992. *Appl. Opt.* 31: 3161–69
Allen, J. G., Jankevics, A., Wormell, D., Schmutz, L. 1987. *Proc. SPIE* 739: 124–28
Angel, J. R. P. 1992. See Fugate 1992a, pp. 494–99
Angel, J. R. P., Wizinowich, P., Lloyd-Hart, M. 1990. *Nature* 348: 221–24
Arsenault, R., Salmon, D. 1992. *CFH Bull.* 27: 8–9
Babcock, H. W. 1953. *Proc. Astron. Soc. Pac.* 65: 229–36
Babcock, H. W. 1958. *J. Opt. Soc. Am.* 48: 500
Babcock, H. W. 1990. *Science* 249: 253–57
Babcock, H. W. 1992. See Fugate 1992a, pp. 1–18
Beckers, J. M. 1987a. *Proc. ICO*–14 (*Quebec*) = *SPIE Proc.* 813: 55–58
Beckers, J. M. 1987b. In *Towards Understanding Galaxies at Large Redshift*, ed. R. Kron, A. Renzini, pp. 319–38. Dordrecht: Kluwer
Beckers, J. M. 1987c. See Merkle et al 1987, pp. 55–85

Beckers, J. M. 1988a. See Ulrich 1988, pp. 693–703
Beckers, J. M. 1988b. See Ulrich 1988, pp. 627–38
Beckers, J. M. 1988c. *Proc. NATO Workshop on "Solar and Stellar Granulation,"* ed. R. J. Rutten, G. Severino, pp. 43–54. Dordrecht: Kluwer
Beckers, J. M. 1989a. In *NOAO proposal to NSF for* 8 *meter Telescopes.* Append. N
Beckers, J. M. 1989b. *Proc. SPIE* 1114: 215–17
Beckers, J. M. 1990. *Proc. SPIE* 1236: 154–63
Beckers, J. M. 1991a. *Exp. Astron.* 2: 57–71
Beckers, J. M. 1991b. *Appl. Opt.* 30: 5010–11
Beckers, J. M. 1992a. *Appl. Opt.* 31: 424–25
Beckers, J. M. 1992b. See Beckers & Merkle 1992. In press.
Beckers, J. M. 1992c. See Ulrich 1992, pp. 497–504
Beckers, J. M. 1992d. See Ulrich 1992, pp. 505–16
Beckers, J. M. 1992e. *Appl. Opt.* 31: 6592–94
Beckers, J. M. 1992f. See Fugate 1992a, pp. 629–38
Beckers, J. M., Goad, L. E. 1987. In *Instrumentation for Ground-Based Optical*

Astronomy, ed. L. Robinson, pp. 315–36. New York: Springer-Verlag

Beckers, J. M., Goad, L. E. 1988. In *Towards Understanding Galaxies at Large Redshift*, ed. R. G. Kron, A. Renzini, pp. 319–38. Dordrecht: Kluwer

Beckers, J. M., Merkle, F. 1989a. *Proc. of Symp. on the JNLT and Related Eng. Dev.*, ed. T. Kogure, A. Tokunaga. *Astrophys. Space Sci.* 160: 345–51

Beckers, J. M., Merkle, F. 1989b. *Proc. SPIE* 1130: 10–16

Beckers, J. M., Merkle, F., eds. 1992. *Proc. of ESO Conf. on "High Resolution Imaging by Interferometry II."* In press

Beckers, J. M., Roddier, F., Eisenhardt P., Shu, K. L. 1986. *Proc. SPIE* 628: 290–97

Beckers, J. M., Williams, J. W. 1979. *MMT Tech. Memo.* 79–1

Bester, M., Danchi, W. C., Degiaccomi, C. G., Greenhill, L. J., Townes, C. H. 1992a. *Ap. J.* In press

Bester, M., Danchi, W. C., Degiaccomi, C. G., Greenhill, L. J., Townes, C. H. 1992b. See Beckers & Merkle 1992. In press

Bonaccini, D., Brusa, G., Esposito, S., Salinari, P., Stefanini, P. 1990. *Proc. SPIE* 1334: 89–97

Bonaccini, D., Brusa, G., Esposito, S., Salinari, P., Stefanini, P. et al. 1991. *Proc. SPIE* 1543: 133–43

Boyer, C., Gaffard, J. 1991. *Proc. SPIE* 1542: 46–61

Boyer, C., Michau, V., Rousset, G. 1990a. *Proc. SPIE* 1237: 406–21

Boyer, C., Michau, V., Rousset, G. 1990b. *Proc. SPIE* 1271: 63–81

Buffington, A., Crawford, F. S., Muller, R. A., Schemin, A. J., Smits, R. G. 1977a. *J. Opt. Soc. Am.* 67: 298–303

Buffington, A., Crawford, F. S., Muller, R. A., Orth, C. D. 1977b. *J. Opt. Soc. Am.* 67: 304–5

Chassat, F. 1989. *J. Optics (Paris)* 20: 13–23

Chassat, F., Rousset, G., Primot, J. 1989a. *Proc. SPIE* 1114: 14–22

Chassat, F., Rousset, G., Primot, J. 1989b. *Proc. SPIE* 1130: 33–41

Clampin, M., Durrance, S. T., Golimowski, D. A., Barkhouser, R. H. 1991. *Proc. SPIE* 1542: 165–74

Colavita, M. M., Shao, M., Staelin, D. H. 1987. *Appl. Opt.* 26: 4106–12

Conan, J. M., Madec, P. Y., Rousset, G. 1992. See Ulrich 1992, pp. 475–78

Coulman, C. E., Vernin, J. 1991. *Appl. Opt.* 30: 118–26

Dicke, R. H. 1982. *Ap. J.* 198: 605–15

Doel, A. P., Dunlop, C. N., Major, J. V., Myers, R. M., Sharples, R. M. 1991a. *Proc. SPIE* 1542: 319–27

Doel, A. P., Dunlop, C. N., Major, J. V.,

Myers, R. M., Sharples, R. M. 1991b. *Proc. SPIE* 1543: 472–78

Doel, A. P., Dunlop, C. N., Major, J. V., Myers, R. M., Sharples, R. M. 1992. See Ulrich 1992, pp. 523–26

Dunn, R. B. 1987a. See Merkle et al 1987, pp. 87–106

Dunn, R. B. 1987b. See Merkle et al 1987, pp. 243–53

Dunn, R. B. 1987c. See Merkle et al 1987, pp. 263–68

Dunn, R. B. 1989. *Bull. Am. Astron. Soc.* 21: 847–48 (Abstr.)

Dunn, R. B. 1990. *Proc. SPIE* 1271: 216–31

Dunn, R. B., Streander, G. W., Hull, W., Wilkins, L. 1991. *Proc. SPIE* 1543: 88–100

Durrance, S. T., Clampin, M. 1989. *Proc. SPIE* 1114: 97–104

Ealey, M. 1991. *Proc. SPIE* 1543: 2–34

Ealey, M. A., Washeba, J. F. 1990. *Opt. Eng.* 29: 1191–98

Ealey, M. A., Wellman, J. A. 1991. *Proc. SPIE* 1543: 36–51

Ellerbroek, B. 1992a. See Fugate 1992a, pp. 441–58

Ellerbroek, B. 1992b. See Ulrich 1992, pp. 411–14

Feinlieb, J. 1982. *Proposal No.* 82-P4. Cambridge: Adaptive Opt. Assoc. (unpubl.)

Fontanella, J.-C. 1985. *J. Opt. (Paris)* 16: 257–68

Fontanella, J.-C., Kern, P., Merkle, F., Gaffard, J.-P., Rousset, G. 1988. *Proc. SPIE* 860: 9–15

Fontanella, J.-C., Rousset, G., Léna, P. 1991. *J. Opt. (Paris)* 22: 99–111

Forbes, F. 1989. *Proc. SPIE* 1114: 146–51

Forbes, F., Roddier, N. 1991. *Proc. SPIE* 1542: 140–47

Foy, R. 1992. See Fugate 1992a, pp. 487–90

Foy, R., Boucher, Y., Fleury, B., Grynberg, G., McCullough, P. R., et al. 1992. See Ulrich 1992, pp. 437–42. In press

Foy, R., Labeyrie, A. 1985. *Astron. Astrophys.* 152: L29–L31

Foy, R., Tallon, M., Séchaud, M., Hubin, N., Brixon, L. 1989. *Proc. SPIE* 1114: 174–83

Fried, D. L. 1982. *J. Opt. Soc. Am.* 72: 52–61

Fugate, R. Q., ed. 1992a. *Laser Guide Star Adaptive Optics Workshop*, Albuquerque, NM. 829 pp.

Fugate, R. Q. 1992b. See Ulrich 1992, pp. 407–10

Fugate, R. Q., Fried, D. L., Ameer, G. A., Boeke, B. R., Browne, S. L., et al. 1991. *Nature* 353: 144–46

Fugate, R. Q., Spinhirne, J. M., Moroney, J. F., Boeke, B. R., Cleis, R. A., et al. 1992. See Fugate 1992a, pp. 132–37

Gaffard, J.-P. 1991. *Proc. SPIE* 1542: 34–45

Gaffard, J.-P., Boyer, C. 1987. *Appl. Opt.* 26: 3772–77

Gaffard, J.-P., Boyer, C. 1989. *Proc. SPIE* 1114: 105–19

Gaffard, J.-P., Boyer, C. 1990. *Proc. SPIE* 1271: 33–50

Gaffard, J.-P., Delanois, G. 1991. *Proc. SPIE* 1542: 34–45

Gardner, C. S., Welsh, B. M., Thompson, L. A. 1989. *Proc. SPIE* 1114: 191–202

Gardner, C. S., Welsh, B. M., Thompson, L. A. 1991. *Proc. IEEE* 78: 1721–43

Gavel, D., Morris, J. R. 1992. See Fugate 1992a, pp. 619–28

Geary, J. C. 1992. See Fugate 1992a, pp. 735–42

Gendron, E., Cuby, J. G., Rigaut, F., Léna, P., Fontanella, J.-C., et al. 1991. *Proc. SPIE* 1542: 297–307

Goad, L. E. 1991. *Proc. SPIE* 1542: 100–9

Goad, L. E., Beckers, J. M. 1989. *Proc. SPIE* 1114: 73–81

Goad, L. E., Roddier, F., Beckers, J. M., Eisenhardt, P. 1986. *Proc. SPIE* 628: 305–13

Golinowski, D. A., Clampin, M., Durrance, S. T. 1992. *Bull. Am. Astron. Soc.* 24: 789 (Abstr.)

Graves, J. E., McKenna, D. L. 1991. *Proc. SPIE* 1542: 262–72

Graves J. E., Roddier, F., McKenna, D., Northcott, M. 1992. See Fugate 1992a, pp. 511–21

Greenaway, A. H. 1991. *Proc. SPIE* 1494: 386–93

Greenaway, A. H. 1992. See Fugate 1992a, pp. 663–68

Greenwood, D. 1977. *J. Opt. Soc. Am.* 67: 390–95

Greenwood, D. P. 1979. *J. Opt. Soc. Am.* 69: 549–53

Greenwood, D. G., Fried, D. L. 1976. *J. Opt. Soc. Am.* 66: 193–206

Grosso, R. P., Yellin, M. 1977. *J. Opt. Soc. Am.* 67: 399–406

Happer, W., MacDonald, G. 1982. *JASON Rep. No. JSR–82–106.* McLean, Virg.: MITRE Corp. (Unpubl.)

Hardy, J. W. 1978. *Proc. IEEE* 66: 651–97

Hardy, J. W. 1980. In *Solar Instrumentation: What's Next?*, ed. R. B. Dunn, pp. 421–33. Sunspot, NM: Sacramento Peak Obs.

Hardy, J. W. 1981. *Scientific Importance of High-Angular Resolution at Infrared and Optical Wavelengths, ESO Conf. Proc.*, pp. 25–39

Hardy, J. W. 1982. *Proc. SPIE* 332: 252–59

Hardy, J. W. 1987. See Merkle et al 1987, pp. 137–54

Hardy, J. W. 1989. *Proc. SPIE* 1114: 2–13

Hardy, J. W. 1991. *Proc. SPIE* 1542: 2–17

Hardy, J. W., Lefebvre, J. E., Koliopoilos, C. L. 1977. *J. Opt. Soc. Am.* 67: 360–69

Hardy, J. W., MacGovern, A. J. 1987. *Proc. SPIE* 816: 180–95

Hogge, C. B., Butts, R. R. 1982. *J. Opt. Soc. Am.* 72: 606–9

Hufnagel, R. E. 1974. *Digest of Tech. Pap., Topical Meet. on Optical Propagation through Turbulence.* Washington, DC: Opt. Soc. Am.

Hulburd, W. G. 1989. *Proc. SPIE* 1130: 42–49

Hulburd, B., Sandler, D. 1990. *Opt. Eng.* 29: 1186–90

Humphreys, R. A., Primmerman, C. A., Bradley, L. C., Herrmann, J. 1991. *J. Opt. Lett.* 16: 1367–69

Humphreys, R. A., Bradley, L. C., Herrmann, J. 1992. *Lincoln Lab. J.* 5: 45–65

Jagourel, P., Madec, P. Y., Séchaud, M. 1990a. *Proc. SPIE* 1237: 394–405

Jagourel, P., Madec, P. Y., Séchaud, M. 1990b. *Proc. SPIE* 1271: 160–71

Jankevics, A. J., Wirth, A. 1991. *Proc. SPIE* 1543: 438–48

Jeys, T. H., Brailove, A. A., Mooradian, A. 1989. *Appl. Opt.* 28: 2588–91

Johnston, D. C., Welsh, B. M. 1991. *Proc. SPIE* 1542: 76–87

Kern, P. 1990. *Optique adaptative et grand télescopes.* Doctoral thesis. Univ. Paris

Kern, P., Léna, P., Rousset, G., Fontanella, J.-C., Merkle, F., et al. 1988. See Ulrich 1988, pp. 657–65

Kern, P., Léna, P., Gigan, P., Fontanella, J.-C., Rousset, G., et al. 1989a. *Proc. SPIE* 1114: 54–64

Kern, P., Léna, P., Gigan, P., Fontanella, J.-C., Rousset, G., et al. 1989b. *Proc. SPIE* 1130: 17–28

Kern, P., Rigaut, F., Léna, P., Merkle, F., Rousset, G. 1990a. *Proc. SPIE* 1237: 345–55

Kern, P., Léna, P., Gigan, P., Rigaut, F., Fontanella, J., et al. 1990b. *Proc. SPIE* 1271: 243–53

Kibblewhite, E. 1992a. See Fugate 1992a, pp. 24–36

Kibblewhite, E. 1992b. See Ulrich 1992, pp. 425–36

Kibblewhite, E., Wild, W. 1992. See Fugate 1992a, pp. 522–34

King, I. R. 1971. *Proc. Astron. Soc. Pac.* 83: 199–201

Kokorovski, S. A. 1979. *J. Opt. Soc. Am.* 69: 181–87

Koliopoulos, C. L. 1980. *Appl. Opt.* 19: 1523–28

Kolmogorov, A. N. 1941. *Dan. SSSR* 30(4): 229

Lloyd-Hart, M., Wizinowich, P., Angel, R., McLeod, B., McCarthy, D., et al. 1992a. See Fugate 1992a, pp. 500–10

Lloyd-Hart, M., Wittman, D., Colucci, D., McLeod, B., Dekany, R., et al. 1992b. See Ulrich 1992, pp. 493–96

Malbet, F. 1992. See Ulrich 1992, pp. 531–34

Malbet, F., Léna, P., Bertout, C. 1991. *The Messenger* 66: 32–33

Malbet, F., Léna, P., Bertout, C. 1992. *Astron. Astrophys.* In press

Mariotti, J.-M., Perrier, C. 1991. *The Messenger* 64: 29–32

Mariotti, J.-M., Perrier, C., Duquennoy, A., Rigaut, F., Gehring, G., et al. 1992. See Beckers & Merkle 1992. In press

Max, C. E, Avicola, K., Bissinger, H., Brase, J., Gavel, D., et al. 1992a. See Ulrich 1992, pp. 443–52

Max, C. E, Avicola, K., Bissinger, H., Brase, J., Gavel, D., et al. 1992b. See Fugate 1992a, pp. 535–41

Megie, G., Bos, F., Blamont, J. E., Chanin, M. L. 1978. *Planet. Space Sci.* 26: 27–35

Merkle, F. 1986. *ESO Conf. and Workshop Proc.* 24: 443–56

Merkle, F. 1987a. See Merkle et al 1987, pp. 35–54

Merkle, F. 1987b. See Merkle et al 1987, pp. 117–30

Merkle, F. 1987c. In *Instrumentation for Ground-Based Optical Astronomy*, ed. L. Robinson, pp. 366–77. New York: Springer-Verlag

Merkle, F. 1988. See Ulrich 1988, pp. 639–56

Merkle, F. 1989a. *Highlights Astron.* 8: 565–66

Merkle, F. 1989b. *Proc. of NATO Workshop on "Diffraction Limited Imaging with Very Large Telescopes,'* ed. J.-M. Mariotti, D. Alloin, pp. 237–48. Dordrecht: Kluwer

Merkle, F. 1991. In *International Trends in Optics*, ed. J. W. Goodman, pp. 375–90. New York: Academic

Merkle, F. 1992a. See Ulrich 1992, pp. 461–70

Merkle, F. 1992b. See Fugate 1992a, pp. 476–86

Merkle, F., Beckers, J. M. 1989. *Proc. SPIE* 1114: 36–42

Merkle, F., Engvold, O., Falomo, R., eds. 1987. *Proc. of LEST Workshop on Adaptive Optics in Solar Observations* (*LEST Tech. Rep. No.* 28). 274 pp.

Merkle, F., Freischlad, K., Reischmann, H. L. 1982. *Proc. SPIE* 332: 260–68

Merkle, F., Gehring, G., Rigaut, F., Léna, P., Rousset, G., et al. 1991a. *Proc. SPIE* 1542: 308–18

Merkle, F., Hubin, N. 1991. *Proc. SPIE* 1542: 283–92

Merkle, F., Hubin, N., Gehring, G., Rigaut, F. 1991b. *The Messenger* 65: 13–14

Merkle, F., Kern, P., Léna, P., Rigaut, F., Fontanella, J.-C., et al. 1989. *The Messenger* 58: 1–5

Merkle, F., Kern, P., Rigaut, F., Léna, P.,

Rousset, G. 1990c. *Proc. SPIE* 1271: 232–42

Merkle, F., Rousset, G., Kern, P., Gaffard, J. 1990a. *Proc. SPIE* 1236: 193–202

Merkle, F., Rousset, G., Kern, P., Gaffard, J. 1990b. *Astron. Astrophys.* 230: L29–L32

Merkle, F., Gehring, G., Rigaut, F., Léna, P., Rousset, G., et al. 1991a. *Proc. SPIE* 1542: 308–18

Murphy, D. V. 1992. *Lincoln Lab. J.* 5: 25–44

Murphy, D. V., Primmerman, C. A., Zollars, B. G., Barclay, H. T. 1991. *Opt. Lett.* 16: 1797–99

Murphy, D. V., Zollars, B. G., Primmerman, C. A. 1992. See Ulrich 1992, pp. 415–18

Nisenson, P., Barakat, R. 1987. *J. Opt. Soc. Am.* A4: 2249–53

Noll, R. J. 1976. *J. Opt. Soc. Am.* 66: 207–11

Northcott, M. J. 1991. *Proc. SPIE* 1542: 254–61

Olivier, S. S., Max, C., Gavel, D. T., Brase, J. M. 1992a. See Fugate 1992a, pp. 567–74

Olivier, S. S., Max, C., Gavel, D. T., Brase, J. M. 1992b. See Ulrich 1992, pp. 489–92

Parenti, R. R. 1992a. *Lincoln Lab. J.* 5: 93–113

Parenti, R. R. 1992b. See Fugate 1992a, pp. 458–75

Parenti, R., Sasiela, R. J. 1992. See Ulrich 1992, pp. 419–24

Peri, M. L., Smithson, R. C., Acton, D. S., Frank, Z. A., Title, A. M. 1988. *Proc. NATO Workshop on "Solar and Stellar Granulation,"* ed. R. J. Rutten, G. Severino, pp. 77–89. Dordrecht: Kluwer

Primmerman, C. A., Murphy, D. V., Page, D. A., Zollars, B. G., Barclay, H. T. 1991. *Nature* 353: 141–43

Rigaut, F., Combes, M., Dougados, C., Léna, P., Mariotti, J.-M., et al. 1992c. See Ulrich 1992, pp. 479–85

Rigaut, F., Cuby, J. G., Caes, M., Monin, J. L., Rousset, G., et al. 1992a. *Astron. Astrophys.* 259: L57–L60

Rigaut, F., Gehring, G. 1992. In preparation

Rigaut, F., Gendron, E. 1992a. See Fugate 1992a, pp. 582–90

Rigaut, F., Gendron, E. 1992b. *Astron. Astrophys.* In press

Rigaut, F., Gendron, E., Léna, P., Madec, P. Y., Couvée, P., et al. 1992b. See Beckers & Merkle 1992. In press

Rigaut, F., Léna, P., Madec, P. Y., Rousset, G., Gendron, E., et al. 1992d. See Ulrich 1992, pp. 399–402

Rigaut, F., Rousset, G., Kern, P., Fontanella, J.-C., Gaffard, J.-P., et al. 1991. *Astron. Astrophys.* 250: 280–90

Roddier, F. 1981. *Prog. Opt.* 19: 281–377

Roddier, F. 1987. See Merkle et al 1987, pp. 7–15

Roddier, F. 1988b. *Appl. Opt.* 27: 1223–25

Roddier, F. 1989. *Proc. of NATO Workshop on "Diffraction Limited Imaging with Very Large Telescopes,"* ed. J.-M. Mariotti, D. Alloin, pp. 33–52. Dordrecht: Kluwer

Roddier, F. 1990. *Opt. Eng.* 29: 1239–42

Roddier, F. 1991. *Proc. SPIE* 1487: 500–10

Roddier, F. 1992a. See Beckers & Merkle 1992. In press

Roddier, F. 1992b. See Fugate 1992a, pp. 19–23

Roddier, F., Eisenhardt, P. 1985. *Proc. SPIE* 556: 248–54

Roddier, F., Eisenhardt, P. 1986. *Proc. SPIE* 628: 314–22

Roddier, F., Forbes, F., Shaklan, S., Pinches, C. 1987. See Merkle et al 1987, pp. 107–16

Roddier, F., Graves, J. E., McKenna, D., Northcott, 1991a. *Proc. SPIE* 1542: 248–53

Roddier, F., Léna, P. 1984. *J. Opt. (Paris)* 15: 363–74

Roddier, F., Northcott, M., Graves, J. E. 1991b. *Proc. Astron. Soc. Pac.* 103: 131–49

Roddier, F., Roddier, C. 1986. *Proc. SPIE* 628: 298–304

Roddier, F., Roddier, C., Roddier, N. 1988. *Proc. SPIE* 976: 203–9

Roddier, F., Roddier, C. 1988. See Ulrich 1988, pp. 667–73

Roddier, N., Roddier, F. 1989. *Proc. SPIE* 1114: 92–96

Roddier, N. 1990. *Opt. Eng.* 29: 1174–80

Roddier, N. 1991. *Proc. SPIE* 1542: 120–29

Roggemann, M. C. 1991. *Appl. Opt.* 30: 4227–33

Rousset, G., Fontanella, J.-C., Kern, P., Gigan, P., Rigaut, F., et al. 1990b. *Astron. Astrophys.* 230: L29–L32

Rousset, G., Fontanella, J.-C., Kern, P., Léna, P., Gigan, P., et al. 1990a. *Proc. SPIE* 1237: 336–44

Rousset, G., Madec, P.-Y., Beuzit, J.-L., Cuby, J.-G., Gigan, P., et al. 1992b. See Ulrich 1992, pp. 403–6

Rousset, G., Madec, Y., Raboud, D. 1992a. See Beckers & Merkle 1992. In press

Rousset, G., Primot, J., Fontanella, J.-C. 1987. See Merkle et al 1987, pp. 17–34

Saint-Pé, O., Combes, M., Rigaut, F., Fulchinioni, M., Tomasko, M. T. 1992. *Icarus* Submitted

Sandler, D. G, Barrett, T. K., Fugate, R. Q. 1991b. *Proc. SPIE* 1543: 491–99

Sandler, D. G., Barrett, T. K., Palmer, D. A., Fugate, R. Q., Wild, W. J. 1991a. *Nature* 351: 300–2

Séchaud. M., Hubin, N., Brixon, L., Jalin, R., Foy, R., et al. 1988. See Ulrich 1988, pp. 705–14

Séchaud, M., Rousset, G., Michau, V., Fontanella, J.-C., Cuby, J. G., et al. 1991. *Proc. SPIE* 1543: 479–91

Shack, R. V., Platt, B. C. 1971. *J. Opt. Soc. Am.* 61: 656 (Abstr.)

Shamir, J., Crowe, D. 1992. See Fugate 1992a, pp. 591–605

Sharples, R., Doel, A. P., Dunlop, C. N., Major, J. V., Myers, R. M. 1992. See Fugate 1992a, pp. 575–81

Smithson, R. C. 1987. *Proc. SPIE* 779: 18–22

Smithson, R. C., Marshall, N. K., Sharbaugh, R. J., Pope, T. P. 1984. In *Small Scale Dynamic Processes in Quiet Stellar Atmospheres*, ed. S. Keil, pp. 66–73. Sunspot, NM: Natl. Sol. Obs.

Smithson, R. C., Peri, M. L. 1987. See Merkle et al 1987, pp. 193–204

Smithson, R. C., Peri, M. L. 1989. *J. Opt. Soc. Am.* A6: 92–97

Smithson, R. C., Peri, M. L., Benson, R. S. 1988. *Appl. Opt.* 27: 1615–20

Steinhaus, E., Lipson, S. G. 1979. *J. Opt. Soc. Am.* 69: 478–81

Tallon, M., Foy, R. 1990. *Astron. Astrophys.* 235: 549–57

Tallon, M., Foy, R., Vernin, J. 1992a. See Fugate 1992a, pp. 555–66

Tallon, M., Foy, R., Vernin, J. 1992b. See Ulrich 1992, pp. 517–22

Tatarski, V. I. 1961. *Wave Propagation in a Turbulent Atmosphere*. New York: Dover

Thompson, L. A., Gardner, C. S. 1987. *Nature* 328: 229–31

Thompson, L. A., Gardner, C. S. 1988. In *Instrumentation for Ground-Based Astronomy*, ed. L. B. Robinson, pp. 337–44. New York: Springer-Verlag

Thompson, L. A., Gardner, C. S. 1989. *Proc. SPIE* 1114: 184–90

Title, A. M., Peri, M. L., Smithson, R. C., Edwards, C. G. 1987. See Merkle et al 1987, pp. 107–16

Tyson, R. K. 1991. *Principles of Adaptive Optics*. New York: Academic. 298 pp.

Ulrich, M.-H., ed. 1988. *Proc. ESP Conf. on Very Large Telescopes and their Instrumentation (ESO Conf. and Workshop Proc. No. 30)*. 1334 pp. Garching, Germany: ESO

Ulrich, M.-H., ed. 1992. *Proc. of ESO Conf. on Progress in Telescope and Instrumentation Technologies*. In press

Valley, G. C. 1980. *Appl. Opt.* 19: 574–577

von der Lühe, O. 1983. *LEST Found. Tech. Rep. No. 2*

von der Lühe, O. 1987. See Merkle et al 1987, pp. 155–67

von der Lühe, O. 1988. *Opt. Eng.* 27: 1078–87

von der Lühe, O. 1991. *Adv. Space Res.* 11: 275–84

Wang, J. Y., Markey, J. K. 1978. *J. Opt. Soc. Am.* 68: 78–87

Welsh, B. M. 1991a. *Appl. Opt.* 30: 5021–30

Welsh, B. M. 1991b. *Proc. SPIE* 1542: 88–100

Welsh, B. M., Gardner, C. S. 1989. *J. Opt. Soc. Am.* A6: 1913–23

Welsh, B. M., Gardner, C. S. 1991. *J. Opt. Soc. Am.* A8: 69–80

Wilson, R. N., Franza, F., Noethe, L. 1987. *J. Mod. Opt.* 34: 485–509

Wirth, A., Ruquist, R. 1985. *Proc. SPIE* 551: 127–30

Wittman, D., Angel, R., McLloyd-Hart, M.,

Colucci, D., McCarthy, D. 1992. See Ulrich 1992, pp. 453–60

Wizinowich, P., Lloyd-Hart, M., McLeod, B. A., Colucci, D., Dekany, R. G., et al. 1991. *Proc. SPIE* 1542: 148–58

Woolf, N. J. 1982. *Annu. Rev. Astron. Astrophys.* 20: 367–98

Woolf, N. J. 1984. *Very Large Telescopes, their Instrumentation and Programs. IAU Colloq. No.* 79, ed. M.-H. Ulrich, K. Kjär, pp. 221–33

Woolf, N. J., Angel, J. R. P, 1980. In *Optical and Infrared Telescopes for the 1980s*, ed. A. Hewitt, pp. 1062–150

Zollars, B. G. 1992. *Lincoln Lab. J.* 5: 67–92

CONTENTS